Science Advances
AAAS
Manuscript Template

FRONT MATTER

Title

A Wearable Textile-Based Pneumatic Energy Harvesting System for Assistive Robotics

Authors

Rachel A. Shveda,[1]† Anoop Rajappan,[1]† Te Faye Yap,[1] Zhen Liu,[1] Marquise D. Bell,[1] Barclay Jumet,[1] Vanessa Sanchez,[2,3] Daniel J. Preston[1]*

Affiliations

[1]Department of Mechanical Engineering, William Marsh Rice University, Houston, TX 77005, USA.

[2]John A. Paulsen School of Engineering and Applied Sciences, Harvard University, Cambridge, MA 02138, USA.

[3]Wyss Institute for Biologically Inspired Engineering, Harvard University, Boston, MA 02115, USA.

*Corresponding author. Email: djp@rice.edu

†These authors contributed equally to this work.

Abstract

Wearable assistive, rehabilitative, and augmentative devices currently require bulky power supplies, often making these tools more of a burden than an asset. This work introduces a soft, low-profile, textile-based pneumatic energy harvesting system that extracts power directly from the foot strike of a user during walking. Energy is harvested with a textile pump integrated into the insole of the user's shoe and stored in a wearable textile bladder to operate pneumatic actuators on demand, with system performance optimized based on a mechano-fluidic model. The system recovered a maximum average power of nearly 3 W with over 20% conversion efficiency—outperforming electromagnetic, piezoelectric, and triboelectric alternatives—and was used to power a wearable arm lift device that assists shoulder motion and a supernumerary robotic arm, demonstrating its capability as a lightweight, low-cost, and comfortable solution to support adults with upper body functional limitations in activities of daily living.

Teaser

A lightweight, wearable textile-based system harvests and stores energy during walking to power pneumatic assistive devices.

MAIN TEXT

Introduction

More than 30 million adults in the United States live with an upper body functional limitation (*1*). The most common limitation reported among adults is difficulty lifting a ten-pound object, with 13 million unable to do so at all, while several million adults also have difficulty grasping, reaching, and pushing or pulling with their hands (*1*). Upper body function is critical to a person's ability to perform activities of daily living such as eating, dressing, and bathing; limited ability to perform these functions correlates with an increased risk of mortality (*2*), and employed adults with a disability earn 25% less than adults without a disability (*1*). Wearable assistive devices that are soft, affordable, low-profile, lightweight, and portable can significantly enhance pathways to recovery and quality of life for individuals with upper body impairments (*3*, *4*).

Various assistive and rehabilitative devices have been designed to support individuals with upper body limitations; these devices include soft exogloves for hand support and rehabilitation (*5*–*7*), exosuits for back support and rehabilitation (*8*, *9*), and exosleeves for shoulder (*10*–*12*), elbow (*13*–*15*), forearm (*16*, *17*), and wrist (*18*–*20*) support and rehabilitation (*21*, *22*). Such devices can also serve to augment the capabilities of non-disabled adults by, for example, acting as a supernumerary limb (or "third arm") (*23*–*27*), supplementing lifting capacity (*28*), or providing hip and ankle assistance during loaded walking (*29*, *30*). Supernumerary robotic limbs, in particular, have been effective in supporting, assisting, or enhancing users' existing capabilities (*31*–*34*). Wearable robotic devices are often made from soft and lightweight materials such as elastomers and textiles to promote comfort and safety of the user (*3*). However, these devices require power, and the weight and bulk of common power supplies such as batteries, compressors, and pumps, as well as accompanying hardware such as valves, cables, and electronics, often make these tools more of a burden than an asset (*35*). The development of lightweight, portable, and unobtrusive power sources is thus a prerequisite for the emergence of practical wearables that fully leverage the capabilities of soft robotic actuators (*35*, *36*).

Integration of energy harvesting capability in clothing offers an attractive substitute for bulky onboard power units and is capable of significantly reducing device weight and size while precluding the need for recharging or refueling as power is generated continuously during use. Body movement, heat, and biochemical potential are all readily available and easily accessible energy sources for wearable devices, with motion of the limbs—specifically, foot strike—representing the most abundant source of power (*37*–*39*). Shoe-based energy harvesting devices have been developed to capitalize on this source of power since as early as 1948 (*40*, *41*). Several physical mechanisms have been used to harvest energy during walking: pneumatic, electromagnetic, triboelectric, piezoelectric, hydroelectric, thermoelectric, and pyroelectric approaches have been demonstrated in prior work (*38*, *39*). Recently, advances in thin-film and fiber-based triboelectric nanogenerators and fiber lithium-ion batteries have enabled their direct integration into shoe insoles and woven textiles (*42*–*44*). However, the power output of these devices is currently in the milliwatt range which, although suitable for sensors and low-power electronics, remains inadequate for powering practical assistive actuators during everyday use. In addition, because many soft actuators used in assistive devices rely on pneumatic actuation (*5*, *45*, *46*), approaches that generate electricity require an additional conversion step from electrical to pneumatic power for use with these assistive devices, further reducing efficiency and adding bulk by requiring more components (*47*, *48*). Ogawa et al. (*49*, *50*) developed an in-shoe pneumatic energy harvesting device, but still relied on a hard tank for pneumatic energy storage; furthermore, their system was neither modeled to elucidate the underlying physics and thermodynamics of operation, nor was it optimized for maximum performance.

In this work, we develop a textile-based energy harvesting system that extracts pneumatic energy using a soft textile pump integrated directly into the insole of the user's shoe; the energy harvested during walking is stored inside a soft, wearable textile bladder until dispensed by the user to power actuators as needed. Our energy harvesting platform thus enables users to comfortably produce and store the power needed to operate the pneumatic actuators found in many common assistive and rehabilitative devices. We built our devices using stacked laminate assembly of heat-sealable textiles, ensuring scalability and ease of manufacturing (*3*, *36*). To optimize the performance of our system, we developed a mechano-fluidic model, validated its predictions against experimental results, and used it to guide the final design of our devices. Our system achieved high conversion efficiencies, recovering more than 20% of the mechanical energy available from walking during experiments; the insole textile pump attained a maximum average power output of 3 W that surpasses the capabilities of existing foot-strike energy harvesting systems based on electrical mechanisms. The direct generation of pneumatic power further eliminates the need for an additional electric-to-pneumatic energy conversion step required by alternate approaches. We demonstrate the use of our system in powering two assistive actuators fabricated entirely from textiles: (i) an arm-lift device that assists shoulder motion, and (ii) a robotic "third arm" that augments user capability.

Results

The textile-based pneumatic energy harvesting system

The soft energy harvesting system comprises two key components each built from textiles: an insole pneumatic pump, which we call the "energy harvesting device" or EHD, and a wearable pneumatic accumulator, which we refer to as the "energy storage bladder" or ESB (Fig. 1). Both the EHD and the ESB were fabricated by first laser patterning and then thermally bonding layers of heat-sealable textile, namely nylon taffeta fabric coated on one side with thermoplastic polyurethane (TPU). Our fabrication approach was guided mainly by the need for scalability and ease of manufacturing of our textile devices; laser patterning allows fast and easy customization of devices, and heat sealing of thermoplastic-coated fabric is a widely adopted technique in the commercial production of garments (*51*). Stacked laminate assembly of carefully designed textile layers yielded durable insole EHDs capable of enduring large applied forces (~ 300 N) and cyclic deformation, and a wearable, low-profile ESB capable of storing air at high pressure (~ 1 bar) with no leakage.

During walking, the compressive force exerted by the user's foot performs mechanical work on the EHD; the EHD converts this work into free energy of pressurized gas, which is then conveyed to and stored in the ESB for later use. To enable its operation as an air pump, we filled the textile pouch of the EHD with water-blown polyurethane foam (Fig. 1A) and added a pair of check valves to enforce unidirectional flow of air from the inlet to the outlet (*52*) (Fig. 1C). When force applied by the foot depresses the EHD (the "foot strike" or compression phase of the pump cycle), air within the pouch is pressurized and forced through the outlet valve into the ESB. When the foot is raised, relieving the force on the EHD (the "liftoff" or intake phase of the pump cycle), the pouch inflates under the restoring force of the foam and is refilled by ambient air drawn through the inlet valve. We fabricated three different prototypes of the EHD, with pouch volumes of 6 mL, 35 mL, and 72 mL; other aspects of the design were kept unchanged. Figure 1C illustrates one possible configuration of the energy harvesting system, and the corresponding placement of the EHD and ESB on the user: the flexible ESB may be worn comfortably around the user's waist, and the soft EHD fits unobtrusively inside the user's shoe. The ESB serves as a portable source of pressurized air for powering pneumatic actuators that assist the user with various functions. The ESB can be repositioned easily, and without affecting system performance, to enhance comfort or facilitate use with commercial assistive and rehabilitative pneumatic devices.

To evaluate the performance of our energy harvesting system, we measured the force of foot strike on the EHD and the pressure inside the ESB as a function of time for a 55 kg user walking on a treadmill at 3 mph (4.8 km/h, corresponding to the average walking speed for adults under 30 years old) (*53*), as shown in Fig. 2A. A video recording of the test using the 35 mL EHD is included as Movie S1. The system successfully extracted and stored pneumatic energy during walking, which was subsequently used to power two textile-based actuators, namely a soft arm-lift assistive device and a supernumerary arm.

Mechano-fluidic modeling of the textile energy harvesting system

We employed a quasi-static force balance on the pouch to model fluid flow through the EHD and thereby characterize its pumping performance (Fig. 2B). To simplify analysis, air inside the pouch was modeled using the ideal gas equation of state, and the temperature of the gas was assumed constant and equal to the steady-state temperature measured inside the shoe. The pumping cycle of the EHD occurs in four consecutive stages as it undergoes repeated loading and unloading inside the shoe. In stage I, force applied during foot strike compresses the EHD and increases the pressure of the gas within the porous foam. When pressure inside the EHD exceeds that of the ESB, the outlet valve opens, releasing compressed air to the ESB for storage (stage II). Stage III commences with liftoff of the foot; as the stepping force is removed, the EHD expands under the restoring force of the foam, and gas pressure inside the pouch falls. Finally, in stage IV, fresh air is drawn in through the intake valve when the internal pressure drops below that of ambient air. The forces acting on the top wall of the pouch (represented by the "piston" of a pneumatic cylinder) at an arbitrary point during this cycle are shown in Fig. 2B; these include the stepping force F_{step} exerted by the foot, the restoring force F_{spring} from the foam, and the pressure forces F_{atm} and F_{gas}, respectively, resulting from internal and external air pressure acting on the effective contact area of the pouch.

Accurate modeling of the pressure within the EHD during the stepping cycle required realistic descriptions of the stepping force, pouch deformation, and reaction force from the foam. To this end, we measured the stepping force on the EHD during walking using force-sensing resistors mounted on the insole of the user's shoe (Fig. S5). The transient force profile could be well-approximated by a trapezoidal waveform with frequency equaling the rate of footfalls during walking (Fig. 2B); the peak force was inferred separately from measurements of the peak gas pressure attained during the compression phase. The flattening of the lenticular EHD pouch when compressed by the foot results in non-linear changes in its internal volume and effective contact area; furthermore, the polyurethane foam behaves as a non-linear spring and its reaction force diverges upon approaching maximum deformation. The change in gas volume as well as the restoring force from the foam were both measured as a function of vertical displacement through simulated compression of the EHD using a universal testing machine (Instron 68SC-2); the internal volume of the EHD was approximated using a quadratic polynomial fit (Fig. S4), whereas the foam reaction force showed good conformance to a neo-Hookean type force function (Fig. S6). We developed a time-stepping routine that solves the non-linear force balance equation numerically to capture the temporal evolution of system parameters—such as the deformation of the EHD and the rate of airflow to the ESB—for any arbitrary choice of the stepping force. A detailed description of our model, including the executable code, is provided in the Supplementary Material. The model predictions for the 6 mL, 35 mL, and 72 mL EHDs are shown alongside experimental data in Figs. 2C and 2D; the predicted pressure traces show good agreement with the experimental pressure measurements for all three prototypes.

We used our mechano-fluidic model to determine the maximum average power (i.e., the maximum power that could be continuously supplied to a balanced load optimized for the system) and the overall energy conversion efficiency of our energy harvesting system. At any given pressure, the usable pneumatic energy stored in the ESB is given by the thermodynamic availability (exergy) of the compressed gas contained within it; the availability is equal to the maximum displacement work that can be extracted if the pressurized gas in the ESB is expanded reversibly against the atmosphere (Eq. S24 and Fig. S7A). To determine the average power output of the EHD, we divided the increase in stored energy during each foot strike by the duration of the corresponding step cycle (Fig. S7B). For a 55 kg human user walking at 3 mph, our system achieved maximum average powers of 2.96 W, 1.94 W, and 0.44 W respectively, using the 72 mL, 35 mL, and 6 mL EHDs (Figs. S7B and S8). In Fig. 2E, we compare the maximum average power output of our system with those achieved by previously reported foot-strike energy harvesting devices based on piezoelectric, triboelectric, and electromagnetic mechanisms (*38*, *50*). The comparison reveals that our system outperforms all approaches utilizing electric mechanisms for energy harvesting by over 100% in maximum average power. Additional details on this comparison with extant foot strike energy harvesting devices are provided in the Supplementary Material (Table S6).

We define the conversion efficiency of our device as the ratio of the energy content of the ESB when it reaches full inflation (taken to be 99% of its final steady-state pressure; see Fig. S9) to the cumulative mechanical work performed by the stepping force on the EHD until that point in time. The work input to the EHD was estimated by integrating the stepping force with respect to the displacement of the foot-pouch contact point; the negative work done by the EHD in raising the foot during the reinflation phase was ignored in this calculation, yielding conservative estimates of efficiency. Our optimized 6 mL EHD achieved an energy conversion efficiency of 23% (details are included in the Supplementary Material).

Validating system performance for different users and walking speeds

Figure 3A shows pneumatic energy harvesting using the 35 mL EHD for a 72 kg user walking at different speeds; whereas 3 mph (4.8 km/h) serves as a typical speed for adults under 30 years of age, a slower speed of about 1 mph (1.6 km/h) may be more accessible for older individuals and users with mobility limitations. We observed that the frequency of footfalls (cadence) does not change significantly with the walking speed; the time interval between successive footfalls decreased only by about 30% (from 1.6 s to 1.1 s) even with a threefold increase in speed (from 1 mph to 3 mph). Consequently, the rate of pressurization of the ESB was independent of speed, as indicated by the collapse of experimental pressure traces when normalized by the terminal ESB pressure (Fig 3B). Furthermore, we observed only a slight (~10%) decrease in the maximum ESB pressure with decrease in speed from 3 mph to 1 mph, which may be attributed to the known reduction in the amplitude of the stepping force at slower speeds (*54*). As neither the final pressure nor the fill rate is sensitive to changes in walking speed within the 1–3 mph range, we believe that our devices may be used effectively at reduced speeds with minimal to no modifications.

We also tested the performance of the 35 mL EHD for five different users with body weights in the range of 52–87 kg (Fig. 4A), walking at a speed of 3 mph; results from these tests are shown in Figs. 4B and 4C. Neglecting small variations that may be attributed to inherent differences in foot size, shoe fit, cadence, and gait between users, we see that the final ESB pressure increases proportionally with the user's body weight on account of the increased maximum heel force exerted on the EHD. This conclusion is further corroborated by our mechano-fluidic model, which predicts a maximum ESB pressure that increases proportionally with the applied heel force (Figs. 4D and 4E). Combining experimental trends (inset to Fig. 4C) with model predictions (Fig. 4E), we infer that approximately 61% of the users' bodyweight is transmitted via their heel to the EHD, which is in excellent agreement with data reported in the literature (*54*).

Powering assistive actuators using harvested pneumatic energy

We demonstrated the ability of our energy harvesting system to generate sufficient energy to operate two pneumatic actuators made entirely of textiles: (i) an arm-lift assistive device (Fig. 5) and (ii) a supernumerary arm (Fig. 6), similar to devices reported in prior work (*25–27*, *55*). Both actuators were again fabricated by stacked laminate assembly of heat-sealable textiles in a process identical to that used for the EHD and ESB (Figs. S2 and S3).

The arm-lift assistive device consists of a pneumatic bellow actuator (*28*, *56*) made of six inflatable textile pouches sewn firmly beneath the shoulder of a long-sleeve compression shirt (Fig. 5A). When pressurized with air from the ESB, the actuator exerts a lifting torque at the shoulder to assist the user in raising (abducting) their arm (Fig. 5B). The number of pouches in the actuator determines the angle through which the arm is raised and the volume of air required per actuation cycle. To quantify the torque generated by the arm-lift device, we employed a mannequin with a freely rotating shoulder joint to preclude all influences of muscular effort when testing on a human user. We varied the supply pressure as well as the weight suspended from the arm (Fig. 5C) and measured the angle of rotation of the shoulder joint to infer the assistive torque (Fig. 5D). Our arm-lift actuator can apply a torque greater than 10 N m (Table S7), which is consistent with the demands on current textile-based assistive devices (*3*). We also demonstrated the use of the arm-lift assistive device, powered solely by energy stored in the ESB, by a human user (Fig. 5A); a video showing the device in operation, on both the mannequin and the human user, is included as Movie S2.

The supernumerary robotic arm (or "third arm") operates using a dual-bladder system (Fig. 6A). The supporting bladder lends mechanical stiffness to the arm during use; it is mounted on the ESB and remains pressurized at all times. The actuating bladder forms the end effector of the arm and, when pressurized, allows the user to grasp and hold objects of various shapes. When not in use, the arm deflates to a compact size and folds conveniently out of the user's way (Fig. 6B). We tested our prototype robotic third arm by utilizing it to grasp common household objects of various sizes, shapes, and weights, including a pair of scissors, a cup, and a granola bar (Figs. 6C and S10); these demonstrations were performed solely using pressurized air generated by the energy harvesting system. Fig. 6D shows a human user picking up a 42.6 g granola bar using the third arm and transporting it to the desired target location 3.5 feet away. Fig. 6E further demonstrates the utility of this device when the user's hands are full, enabling them to pick up and transport a piece of crumpled paper while also holding two large boxes. Operation of the third arm in this work is powered solely by energy harvested with the EHD and stored in the ESB; a video of these demonstrations is included as Movie S3.

Discussion

This work demonstrates a soft, low profile, and comfortable textile-based system that harvests energy during walking to operate pneumatic assistive and rehabilitative devices. A smaller EHD volume results in a slower fill rate but achieves a higher maximum pressure of air stored in the ESB; conversely, a larger EHD volume yields a faster fill rate but achieves a lower maximum pressure (Fig. S9). This behavior occurs because the terminal ESB pressure is determined by the maximum pressure attained in the EHD; the latter, as per the force balance described by Eq. S6, is set by the ratio of the net maximum force on the pouch wall (i.e., the peak heel force minus the spring force) to the effective contact area between the pouch and the foot. For a given heel force, therefore, a smaller

EHD yields a higher maximum pressure due to the smaller contact area through which this force is exerted on the pouch wall. This inverse relationship between EHD size and maximum pressure is further corroborated by the predictions of our mechano-fluidic model, as seen in Fig. 2D. On the other hand, a larger EHD volume enables a faster fill rate on account of the greater quantity of gas pumped during each step cycle. The peak operating pressure and the rate of pressurization can be customized, respectively, by modifying the size of the EHD and the ESB, allowing fine-tuning of the energy harvesting system to meet the needs of the user. Our mechano-fluidic model simplifies device optimization by permitting exploration of the design space of possible EHD and ESB configurations before actual fabrication and testing. The textile-based energy harvesting system can thus be tailored, in principle, to support a variety of existing or future pneumatic actuators and soft wearables that users may need to support or augment their capabilities.

Our pneumatic energy harvesting system is not without limitations. For instance, the maximum energy that our device can supply in a single rapid draw is limited by the internal volume of the ESB. System capacity may be enhanced by enlarging the ESB, or more appropriately, by sizing the ESB commensurate with the maximum energy demand expected from various assistive actuators. For routine use, we envision sizing the components such that the ESB would enable several actuation cycles in quick succession before the user must wait for the EHD to replenish the expended gas. Although our system is well-suited for powering pneumatic actuators directly, some users may still require actuators or controllers powered electrically, necessitating an onboard generator that runs on compressed air. Fortunately, this conversion step can be completed with an efficiency of approximately 50% (*57*), yielding a maximum average power output of about 1.5 W which is still competitive with the maximum values reported for direct harvesting of electrical energy from walking (*38*).

All five users who tested our device reported that the EHD felt comfortable during walking, and most users found its firmness comparable to that of commercial insoles or shoe inserts. While the presence of the device inside the shoe was perceptible, none of the users reported discomfort, pain, or soreness after tests. A systematic investigation of user comfort and ergonomics will be helpful in guiding future optimization of our EHD design to minimize its influence on the user's gait and preclude any possibility of injury from long term use. We believe that balancing user effort across the gait cycle by providing EHDs inside both shoes, as well as reshaping the EHDs to support the full area of each foot, will enhance both user comfort and the efficiency of our energy harvesting system. Another useful feature could be the provision of a valve to disconnect the EHD from the ESB, allowing the user to manually disable energy harvesting if desired.

In summary, the textile-based energy harvesting system developed in this work will support individuals with upper body functional limitations by powering assistive wearables that facilitate activities of daily living, thereby enabling improved quality of life and lowering barriers to social participation. An assessment of our system showed that it outperformed all other foot strike energy harvesting techniques relying on electric mechanisms by over 100% in maximum average power. During experiments, a maximum average power output of nearly 3 W was achieved, and an energy conversion efficiency of 23% was demonstrated. Our current system may be used directly by users with different walking speeds or body weights without design modification. Furthermore, our mechano-fluidic model—which we derived from first principles based on a fundamental thermodynamic and fluidic analysis of our system and validated against experimental results—allows further optimization of power, efficiency, and output characteristics to suit the needs of specific users. Our choice of structural materials, namely heat-sealable textiles and foam, renders our devices soft, portable, and affordable, requiring only $20 in materials to produce all wearable components. The fully assembled system weighs 140 g, which is less than one-tenth of the weight of the power and control infrastructure required to operate a similar textile-based supernumerary arm in prior work (*25*). Unlike expendable energy sources such as single-use battery packs, our device is capable of continuous power generation, eliminating the need for periodic replacement or refueling. Additionally, the fabrication process is simple and inexpensive, and employs off-the-shelf textile materials and well-developed processes such as heat sealing that may be readily scaled for mass production. We are therefore optimistic that our textile-based system can provide a lightweight, low-cost solution for powering wearable devices that will advance the state of the art beyond the limitations imposed by heavy and bulky power sources which serve the current generation of assistive and rehabilitative technologies.

Materials and Methods

Experimental design

The goals of this work are twofold: (a) design a soft, wearable textile-based system for capturing pneumatic energy during walking, and (b) develop an accurate mechano-fluidic model, validated against experimental data, that can be used to predict and optimize system performance. We also demonstrated two textile-based assistive devices—an assistive device to aid shoulder motion and a supernumerary robotic arm— highlighting the ability of our system to meet the requirements of practical assistive and rehabilitative actuators for users with functional limitations. All our devices are textile-based with the goal of enabling lightweight, unobtrusive, and comfortable wearable system. To allow scalability and facilitate replication of our work, we fabricated all devices from commercially available, inexpensive materials.

Fabrication of the insole EHD

Three different EHD prototypes were fabricated with pouch volumes of 6 mL, 35 mL, and 72 mL, respectively; dimensions of the pouches were chosen to fit comfortably and unobtrusively inside the user's shoe. A desktop laser engraver (K40, Orion Motor Tech) was used to cut the outer layers of heat-sealable textile (FHST, TPU-coated nylon taffeta, Seattle Fabrics Inc.) and an inner layer of silicone-coated non-stick textile (FRC13, 1.3 oz silicone impregnated ripstop, Seattle Fabrics Inc.) as shown in Fig. 1A. The layers were stacked, aligned, then heat sealed using a benchtop heat press (DK20SP, Geo Knight) at a temperature of 208 °C and cylinder air pressure of 50 psi for a duration of 30 seconds. Next, a water-blown polyurethane foam mixture (FlexFoam-iT! X, Smooth-On) was prepared and a premeasured quantity of the mixture, calibrated to achieve the intended pouch volume after expansion, was injected into the textile pouch using a syringe (Fig. 1A). The foam was allowed to expand to its final volume and fully cure over a period of at least two hours. Finally, pneumatic connections were glued to the EHD using flexible rubber tubing (9776T1, McMaster-Carr) and check valves were added. The completed EHD is shown in Fig. 1B. Each of the three EHD prototypes weighed less than 27 g and cost less than $3 to fabricate (even when estimated using retail prices; see Table S1).

Fabrication of the wearable ESB

The ESB was designed with an internal volume of approximately 744 mL, distributed across four bladder arrays that were pneumatically linked in series via soft rubber tubing (Fig. S1). The textile bladders were formed by laser patterning and heat sealing TPU-coated nylon taffeta fabric by a process identical to that employed for the EHD. A computerized sewing machine (SQ9285, Brother) was used to stitch the bladder array into a wearable belt by adding elastic as well as hook-and-loop ("Velcro") attachments. Lastly, soft rubber tubing (9776T1, McMaster-Carr) was glued to the bladders to form pneumatic lines and to interconnect different sections of the bladder array. The completed ESB is shown in Fig. 1C; it weighed 91 g and cost $3 to fabricate (even when estimated using retail prices; see Table S2).

The multi-bladder design of the ESB was specifically chosen to avoid pressure on the user's body during use; the hook-and-loop fasteners and elastic strips permit an adjustable and comfortable fit that accommodates users with different waist sizes, without restricting their range of motion or breathing. Once the bladders are fully inflated at ambient pressure, the ESB behaves as a constant volume tank; pressurization of the stored gas during walking causes no further lateral contraction of the bladders, precluding any feeling of constriction or discomfort to the user.

Assembly of the energy harvesting system

Two miniature plastic check valves (C-116B-SI-PS, Industrial Specialties Manufacturing) were attached to the EHD to enable its pumping action. The valves were configured to permit unidirectional airflow either (i) from the atmosphere to the EHD, or (ii) from the EHD to the ESB (Fig. 1C). We used soft and flexible EPDM rubber tubing (durometer hardness 60A, minimum bend radius less than ¼") to convey pressurized air from the outlet of the insole EHD to the inlet of the ESB (worn at the hip level), and from the ESB to various assistive devices. Tubes were routed along the user's garment using miniature hook and loop attachments to prevent kinking due to leg motion. User-controlled actuation of assistive devices was accomplished using a three-way valve (62475K42, Master-Carr) for inflating and deflating the pneumatic end effectors. The assembled system is shown in Fig. 1C; the overall system weighed 136 g and cost $21 to fabricate (even when estimated using retail prices; see Table S3).

Fabrication of the arm-lift assistive device

The bellow actuator—consisting of six inflatable textile pouches—was formed by stacking and heat sealing 16 layers of TPU-coated nylon taffeta (FHST, Seattle Fabrics Inc.) interspersed with 13 layers of non-stick silicone-impregnated ripstop (FRC13, Seattle

Fabrics Inc.), as shown in Fig. S2. Heat sealing was performed using a benchtop heat press (DK20SP, Geo Knight) at a temperature of 200 °C, cylinder pressure of 80 psi, and for a duration of 80 seconds. A computerized sewing machine (SQ9285, Brother) was then used to firmly attach the bellow actuator under the arm of a long-sleeve compression shirt (Figs. 3A and S2). Lastly, soft rubber tubing (9776T1, McMaster-Carr) was glued to the device to provide pneumatic connection to the control valve. The arm-lift assistive device (including the compression shirt) weighed 113 g and cost less than \$23 to fabricate (even when estimated using retail prices; see Table S4). For the experiment shown in Fig. 5C, we used a manual pressure regulator to vary the input pressure to the arm-lift and thereby modulate the angular displacement of the arm.

Fabrication of the supernumerary robotic arm

We built two prototype third-arm devices—a 30 cm “long” version, as well as an 18 cm “short” version—each consisting of two inflatable textile bladders: one for support and the other for actuating the gripper. Figure 4 shows the long arm in operation, whereas additional results for the short arm are included in Fig. S10. Both devices were made by heat sealing 3 layers each of TPU-coated nylon taffeta (FHST, Seattle Fabrics Inc.), interspersed with 2 layers each of non-stick silicone-impregnated ripstop (FRC13, Seattle Fabrics Inc.), as shown in Fig. S3. Heat sealing was performed using a benchtop heat press (DK20SP, Geo Knight) at a temperature of 208 °C, pressure of 60 psi, and for a duration of 40 seconds. A computerized sewing machine (SQ9285, Brother) was then used to add the textile frame supporting the cantilevered arm and to affix a loop attachment point to the wearable ESB (Fig. S3). Separate pneumatic connections to the support and actuating bladders were made using soft rubber tubing (9776T1, McMaster-Carr). The actuating bladder was connected to the three-way valve for controlled actuation of the supernumerary arm, whereas the support bladder was directly fed from the ESB through a check valve (C-116B-SI-PS, Industrial Specialties Manufacturing) to prevent deflation during operation. Lastly, a thin layer of a soft and tacky elastomer (Ecoflex GEL, Smooth-On) was applied to the gripping surface of the arm to improve grip on objects with smooth and slippery surfaces. The short and long third arm devices weighed 9 g and 14 g, respectively, and cost \$8 each to fabricate (Table S5).

Experimental evaluation of the performance of the energy harvesting system

Experimental measurements of system performance were conducted with users walking on a treadmill (TR150, Xterra Fitness). We tested our device with users of different body weights (52–87 kg), who were all authors of this work. Except for data shown in Fig. 3, tests were performed at a speed of 3 mph, corresponding to the average walking speed for users under 30 years old (*53*) (Fig. 2A). For each test, the user walked on the treadmill at a steady pace until the wearable tank was fully inflated. The stepping force applied on the insole EHD during walking was recorded using a force-sensing resistor (FSR 406, Interlink Electronics) mounted inside the user’s shoe and connected to a voltage divider circuit and an analog voltage acquisition system (USB-6211, National Instruments) as shown in Fig. S5. The gas pressure at the inlet of the ESB was monitored using a pressure sensor (ADP5151, Panasonic), also connected to an analog data acquisition system (NI USB-6002, National Instruments).

References

1. D. M. Taylor, Americans with Disabilities: 2014. *Curr. Popul. Reports*, 1–32 (2018).
2. I. M. Majer, W. J. Nusselder, J. P. Mackenbach, B. Klijs, P. H. M. van Baal, Mortality Risk Associated With Disability: A Population-Based Record Linkage Study. *Am. J. Public Health*. **101**, e9–e15 (2011).
3. V. Sanchez, C. J. Walsh, R. J. Wood, Textile Technology for Soft Robotic and Autonomous Garments. *Adv. Funct. Mater.* **31**, 2008278 (2021).
4. P. E. Dupont, B. J. Nelson, M. Goldfarb, B. Hannaford, A. Menciassi, M. K. O'Malley, N. Simaan, P. Valdastri, G.-Z. Yang, A decade retrospective of medical robotics research from 2010 to 2020. *Sci. Robot.* **6** (2021).
5. C.-Y. Chu, R. M. Patterson, Soft robotic devices for hand rehabilitation and assistance: a narrative review. *J. Neuroeng. Rehabil.* **15**, 9 (2018).
6. P. Polygerinos, Z. Wang, K. C. Galloway, R. J. Wood, C. J. Walsh, Soft robotic glove for combined assistance and at-home rehabilitation. *Rob. Auton. Syst.* **73**, 135–143 (2015).
7. H. In, B. B. Kang, M. Sin, K.-J. Cho, Exo-Glove: A Wearable Robot for the Hand with a Soft Tendon Routing System. *IEEE Robot. Autom. Mag.* **22**, 97–105 (2015).
8. G. Agarwal, M. A. Robertson, H. Sonar, J. Paik, Design and Computational Modeling of a Modular, Compliant Robotic Assembly for Human Lumbar Unit and Spinal Cord Assistance. *Sci. Rep.* **7**, 14391 (2017).
9. D. Govin, L. Saenz, G. Athanasaki, L. Snyder, P. Polygerinos, Design and Development of a Soft Robotic Back Orthosis, in *2018 Design of Medical Devices Conference* (American Society of Mechanical Engineers, 2018).
10. C. T. O'Neill, N. S. Phipps, L. Cappello, S. Paganoni, C. J. Walsh, A soft wearable robot for the shoulder: Design, characterization, and preliminary testing, in *2017 International Conference on Rehabilitation Robotics (ICORR)* (IEEE, 2017), pp. 1672–1678.
11. R. F. Natividad, C. H. Yeow, Development of a soft robotic shoulder assistive device for shoulder abduction, in *2016 6th IEEE International Conference on Biomedical Robotics and Biomechatronics (BioRob)* (IEEE, 2016), pp. 989–993.
12. C. S. Simpson, A. M. Okamura, E. W. Hawkes, Exomuscle: An inflatable device for shoulder abduction support, in *2017 IEEE International Conference on Robotics and Automation (ICRA)* (IEEE, 2017), pp. 6651–6657.
13. T. H. Koh, N. Cheng, H. K. Yap, C.-H. Yeow, Design of a Soft Robotic Elbow Sleeve with Passive and Intent-Controlled Actuation. *Front. Neurosci.* **11**, 597 (2017).
14. V. Oguntosin, W. S. Harwin, S. Kawamura, S. J. Nasuto, Y. Hayashi, Development of a wearable assistive soft robotic device for elbow rehabilitation, in *2015 IEEE International Conference on Rehabilitation Robotics (ICORR)* (IEEE, 2015), pp. 747–752.
15. D. Chiaradia, M. Xiloyannis, C. W. Antuvan, A. Frisoli, L. Masia, Design and embedded control of a soft elbow exosuit, in *2018 IEEE International Conference on Soft Robotics (RoboSoft)* (IEEE, 2018), pp. 565–571.
16. J. Realmuto, T. Sanger, A robotic forearm orthosis using soft fabric-based helical actuators, in *2019 2nd IEEE International Conference on Soft Robotics (RoboSoft)* (IEEE, 2019), pp. 591–596.
17. S.-H. Park, J. Yi, D. Kim, Y. Lee, H. S. Koo, Y.-L. Park, A Lightweight, Soft Wearable Sleeve for Rehabilitation of Forearm Pronation and Supination, in *2019 2nd IEEE International Conference on Soft Robotics (RoboSoft)* (IEEE, 2019), pp. 636–641.
18. N. W. Bartlett, V. Lyau, W. A. Raiford, D. Holland, J. B. Gafford, T. D. Ellis, C. J. Walsh,

A Soft Robotic Orthosis for Wrist Rehabilitation. *J. Med. Devices* **9**, 030918 (2015).

19. D. Serrano, D.-S. Copaci, L. Moreno, D. Blanco, SMA based wrist exoskeleton for rehabilitation therapy, in *2018 IEEE/RSJ International Conference on Intelligent Robots and Systems (IROS)* (IEEE, 2018), pp. 2318–2323.
20. B. W. K. Ang, C.-H. Yeow, Design and Characterization of a 3D Printed Soft Robotic Wrist Sleeve with 2 DoF for Stroke Rehabilitation, in *2019 2nd IEEE International Conference on Soft Robotics (RoboSoft)* (IEEE, 2019), pp. 577–582.
21. M. A. Gull, S. Bai, T. Bak, A Review on Design of Upper Limb Exoskeletons. *Robotics* **9**, 16 (2020).
22. S. Lessard, P. Pansodtee, A. Robbins, J. M. Trombadore, S. Kurniawan, M. Teodorescu, A Soft Exosuit for Flexible Upper-Extremity Rehabilitation. *IEEE Trans. Neural Syst. Rehabil. Eng.* **26**, 1604–1617 (2018).
23. P. H. Nguyen, C. Sparks, S. G. Nuthi, N. M. Vale, P. Polygerinos, Soft Poly-Limbs: Toward a New Paradigm of Mobile Manipulation for Daily Living Tasks. *Soft Robot.* **6**, 38–53 (2019).
24. P. H. Nguyen, I. B. Imran Mohd, C. Sparks, F. L. Arellano, W. Zhang, P. Polygerinos, Fabric Soft Poly-Limbs for Physical Assistance of Daily Living Tasks, in *2019 International Conference on Robotics and Automation (ICRA)* (IEEE, 2019), pp. 8429–8435.
25. X. Liang, H. Cheong, C. K. Chui, C.-H. Yeow, A Fabric-Based Wearable Soft Robotic Limb. *J. Mech. Robot.* **11**, 031003 (2019).
26. X. Liang, H. K. Yap, J. Guo, R. C. H. Yeow, Y. Sun, C. K. Chui, Design and characterization of a novel fabric-based robotic arm for future wearable robot application, in *2017 IEEE International Conference on Robotics and Biomimetics (ROBIO)* (IEEE, 2017), pp. 367–372.
27. X. Liang, H. Cheong, Y. Sun, J. Guo, C. K. Chui, C.-H. Yeow, Design, Characterization, and Implementation of a Two-DOF Fabric-Based Soft Robotic Arm. *IEEE Robot. Autom. Lett.* **3**, 2702–2709 (2018).
28. C. M. Thalman, Q. P. Lam, P. H. Nguyen, S. Sridar, P. Polygerinos, A Novel Soft Elbow Exosuit to Supplement Bicep Lifting Capacity, in *2018 IEEE/RSJ International Conference on Intelligent Robots and Systems (IROS)* (IEEE, 2018), pp. 6965–6971.
29. F. A. Panizzolo, I. Galiana, A. T. Asbeck, C. Siviy, K. Schmidt, K. G. Holt, C. J. Walsh, A biologically-inspired multi-joint soft exosuit that can reduce the energy cost of loaded walking. *J. Neuroeng. Rehabil.* **13**, 43 (2016).
30. Y. Ding, F. A. Panizzolo, C. Siviy, P. Malcolm, I. Galiana, K. G. Holt, C. J. Walsh, Effect of timing of hip extension assistance during loaded walking with a soft exosuit. *J. Neuroeng. Rehabil.* **13**, 87 (2016).
31. M. Al-Sada, T. Höglund, M. Khamis, J. Urbani, T. Nakajima, Orochi: Investigating Requirements and Expectations for Multipurpose Daily Used Supernumerary Robotic Limbs, in *Proceedings of the 10th Augmented Human International Conference 2019* (ACM, New York, NY, USA, 2019), pp. 1–9.
32. B. Llorens - Bonilla, F. Parietti, H. H. Asada, Demonstration-based control of supernumerary robotic limbs, in *2012 IEEE/RSJ International Conference on Intelligent Robots and Systems* (IEEE, 2012), pp. 3936–3942.
33. F. Wu, H. Asada, Supernumerary Robotic Fingers: An Alternative Upper-Limb Prosthesis, in *Volume 2: Dynamic Modeling and Diagnostics in Biomedical Systems; Dynamics and Control of Wind Energy Systems; Vehicle Energy Management Optimization; Energy Storage, Optimization; Transportation and Grid Applications; Estimation and Identification Method* (American Society of Mechanical Engineers, 2014), V002T16A009.
34. I. Hussain, G. Salvietti, G. Spagnoletti, M. Malvezzi, D. Cioncoloni, S. Rossi, D.

Prattichizzo, A soft supernumerary robotic finger and mobile arm support for grasping compensation and hemiparetic upper limb rehabilitation. *Rob. Auton. Syst.* **93**, 1–12 (2017).
35. A. Rajappan, B. Jumet, D. J. Preston, Pneumatic soft robots take a step toward autonomy. *Sci. Robot.* **6**, 1–3 (2021).
36. B. Jumet, M. D. Bell, V. Sanchez, D. J. Preston, A Data-Driven Review of Soft Robotics. *Adv. Intell. Syst.* **4**, 2100163 (2021).
37. T. Starner, J. Paradiso, Human-Generated Power for Mobile Electronics, in *Low-Power Electronics Design*, C. Piguet, Ed. (CRC Press, 2004), ch. 45.
38. Y.-M. Choi, M. Lee, Y. Jeon, Wearable Biomechanical Energy Harvesting Technologies. *Energies* **10**, 1483 (2017).
39. H. Shi, Z. Liu, X. Mei, Overview of Human Walking Induced Energy Harvesting Technologies and Its Possibility for Walking Robotics. *Energies*. **13**, 86 (2019).
40. F. A. Matulch, Foot actuated pressure generator. U.S. Patent 2,435,928 (1948).
41. S. R. Anton, H. A. Sodano, A review of power harvesting using piezoelectric materials (2003–2006). *Smart Mater. Struct.* **16**, R1–R21 (2007).
42. S. Niu, X. Wang, F. Yi, Y. S. Zhou, Z. L. Wang, A universal self-charging system driven by random biomechanical energy for sustainable operation of mobile electronics. *Nat. Commun.* **6**, 8975 (2015).
43. J. Chen, Y. Huang, N. Zhang, H. Zou, R. Liu, C. Tao, X. Fan, Z. L. Wang, Micro-cable structured textile for simultaneously harvesting solar and mechanical energy. *Nat. Energy* **1**, 16138 (2016).
44. J. He, C. Lu, H. Jiang, F. Han, X. Shi, J. Wu, L. Wang, T. Chen, J. Wang, Y. Zhang, H. Yang, G. Zhang, X. Sun, B. Wang, P. Chen, Y. Wang, Y. Xia, H. Peng, Scalable production of high-performing woven lithium-ion fibre batteries. *Nature* **597**, 57–63 (2021).
45. T. Shahid, D. Gouwanda, S. G. Nurzaman, A. A. Gopalai, Moving toward Soft Robotics: A Decade Review of the Design of Hand Exoskeletons. *Biomimetics* **3**, 17 (2018).
46. P. Polygerinos, N. Correll, S. A. Morin, B. Mosadegh, C. D. Onal, K. Petersen, M. Cianchetti, M. T. Tolley, R. F. Shepherd, Soft Robotics: Review of Fluid-Driven Intrinsically Soft Devices; Manufacturing, Sensing, Control, and Applications in Human-Robot Interaction. *Adv. Eng. Mater.* **19**, 1700016 (2017).
47. D. J. Preston, P. Rothemund, H. J. Jiang, M. P. Nemitz, J. Rawson, Z. Suo, G. M. Whitesides, Digital logic for soft devices. *Proc. Natl. Acad. Sci.* **116**, 7750–7759 (2019).
48. D. J. Preston, H. J. Jiang, V. Sanchez, P. Rothemund, J. Rawson, M. P. Nemitz, W. Lee, Z. Suo, C. J. Walsh, G. M. Whitesides, A soft ring oscillator. *Sci. Robot.* **4**, eaaw5496 (2019).
49. K. Ogawa, C. Thakur, T. Ikeda, T. Tsuji, Y. Kurita, Development of a pneumatic artificial muscle driven by low pressure and its application to the unplugged powered suit. *Adv. Robot.* **31**, 1135–1143 (2017).
50. K. Ogawa, T. Ikeda, Y. Kurita, Unplugged Powered Suit for Superhuman Tennis, in *2018 12th France-Japan and 10th Europe-Asia Congress on Mechatronics* (IEEE, 2018), pp. 361–364.
51. I. Jones, The use of heat sealing, hot air and hot wedge to join textile materials, in *Joining Textiles*, I. Jones, G. K. Stylios, Eds. (Woodhead Publishing, 2013), ch. 11, pp. 355–373.
52. R. S. Diteesawat, T. Helps, M. Taghavi, J. Rossiter, Electro-pneumatic pumps for soft robotics. *Sci. Robot.* **6** (2021).
53. M. Schimpl, C. Moore, C. Lederer, A. Neuhaus, J. Sambrook, J. Danesh, W. Ouwehand, M. Daumer, Association between Walking Speed and Age in Healthy, Free-Living Individuals Using Mobile Accelerometry—A Cross-Sectional Study. *PLoS One*. **6**, e23299 (2011).
54. P. R. Cavanagh, M. M. Rodgers, A. Liboshi, Pressure Distribution under Symptom-Free

Feet during Barefoot Standing. *Foot Ankle*. **7**, 262–278 (1987).
55. J. Fang, J. Yuan, M. Wang, L. Xiao, J. Yang, Z. Lin, P. Xu, L. Hou, Novel Accordion-Inspired Foldable Pneumatic Actuators for Knee Assistive Devices. *Soft Robot.* **7**, 95–108 (2020).
56. P. H. Nguyen, W. Zhang, Design and Computational Modeling of Fabric Soft Pneumatic Actuators for Wearable Assistive Devices. *Sci. Rep.* **10**, 9638 (2020).
57. D. Krähenbühl, C. Zwyssig, H. Weser, J. W. Kolar, Theoretical and experimental results of a mesoscale electric power generation system from pressurized gas flow. *J. Micromechanics Microengineering*. **19**, 094009 (2009).
58. J. Hayashida, thesis, Massachusetts Institute of Technology (2000).
59. M. Duffy, D. Carroll, Electromagnetic generators for power harvesting, in *2004 IEEE 35th Annual Power Electronics Specialists Conference (IEEE Cat. No.04CH37551)* (IEEE, 2004), pp. 2075–2081.
60. Y. Rao, S. Cheng, D. P. Arnold, An energy harvesting system for passively generating power from human activities. *J. Micromechanics Microengineering*. **23**, 114012 (2013).
61. J.-X. Shen, C.-F. Wang, P. C.-K. Luk, D.-M. Miao, D. Shi, C. Xu, A Shoe-Equipped Linear Generator for Energy Harvesting. *IEEE Trans. Ind. Appl.* **49**, 990–996 (2013).
62. L. Xie, M. Cai, An In-Shoe Harvester With Motion Magnification for Scavenging Energy From Human Foot Strike. *IEEE/ASME Trans. Mechatronics*. **20**, 3264–3268 (2015).
63. A. M. Purwadi, S. Parasuraman, M. K. A. A. Khan, I. Elamvazuthi, Development of Biomechanical Energy Harvesting Device Using Heel Strike. *Procedia Comput. Sci.* **76**, 270–275 (2015).
64. K. Ylli, D. Hoffmann, A. Willmann, P. Becker, B. Folkmer, Y. Manoli, Energy harvesting from human motion: exploiting swing and shock excitations. *Smart Mater. Struct.* **24**, 025029 (2015).
65. L. Xie, J. Li, S. Cai, X. Li, Design and experiments of a self-charged power bank by harvesting sustainable human motion. *Adv. Mech. Eng.* **8**, 168781401665137 (2016).
66. S. Wu, P. C. K. Luk, C. Li, X. Zhao, Z. Jiao, Y. Shang, An electromagnetic wearable 3-DoF resonance human body motion energy harvester using ferrofluid as a lubricant. *Appl. Energy*. **197**, 364–374 (2017).
67. Z. Li, X. Jiang, Y. Peng, J. Luo, S. Xie, H. Pu, Design and Experimental Studies of a Heel-Embedded Energy Harvester for Self-Powered Wearable Electronics, in *ASME 2021 Conference on Smart Materials, Adaptive Structures and Intelligent Systems* (American Society of Mechanical Engineers, 2021), V001T04A006.
68. N. S. Shenck, J. A. Paradiso, Energy scavenging with shoe-mounted piezoelectrics. *IEEE Micro*. **21**, 30–42 (2001).
69. C. A. Howells, Piezoelectric energy harvesting. *Energy Convers. Manag.* **50**, 1847–1850 (2009).
70. J. G. Rocha, L. M. Goncalves, P. F. Rocha, M. P. Silva, S. Lanceros-Mendez, Energy Harvesting From Piezoelectric Materials Fully Integrated in Footwear. *IEEE Trans. Ind. Electron.* **57**, 813–819 (2010).
71. J. Zhao, Z. You, A Shoe-Embedded Piezoelectric Energy Harvester for Wearable Sensors. *Sensors* **14**, 12497–12510 (2014).
72. R. Meier, N. Kelly, O. Almog, P. Chiang, A piezoelectric energy-harvesting shoe system for podiatric sensing, in *2014 36th Annual International Conference of the IEEE Engineering in Medicine and Biology Society* (IEEE, 2014), pp. 622–625.
73. W.-S. Jung, M.-J. Lee, M.-G. Kang, H. G. Moon, S.-J. Yoon, S.-H. Baek, C.-Y. Kang, Powerful curved piezoelectric generator for wearable applications. *Nano Energy* **13**, 174–181 (2015).
74. H. Kalantarian, M. Sarrafzadeh, Pedometers Without Batteries: An Energy Harvesting

Shoe. *IEEE Sens. J.* **16**, 1–1 (2016).
75. K. Fan, Z. Liu, H. Liu, L. Wang, Y. Zhu, B. Yu, Scavenging energy from human walking through a shoe-mounted piezoelectric harvester. *Appl. Phys. Lett.* **110**, 143902 (2017).
76. A. C. Turkmen, C. Celik, Energy harvesting with the piezoelectric material integrated shoe. *Energy* **150**, 556–564 (2018).
77. P. Chaudhary, P. Azad, Energy Harvesting Using Shoe Embedded with Piezoelectric Material. *J. Electron. Mater.* **49**, 6455–6464 (2020).
78. M. Ramalingam, E. Chinnavan, R. Puviarasi, N. H. Yu, Assistive technology for harvesting footstep energy in IoT enabled Smart shoe for the visually impaired, in *2021 International Conference on Software Engineering & Computer Systems and 4th International Conference on Computational Science and Information Management (ICSECS-ICOCSIM)* (IEEE, 2021), pp. 115–118.
79. N. Wang, R. Daniels, L. Connelly, M. Sotzing, C. Wu, R. Gerhard, G. A. Sotzing, Y. Cao, All-Organic Flexible Ferroelectret Nanogenerator with Fabric-Based Electrodes for Self-Powered Body Area Networks. *Small* **17**, 2103161 (2021).
80. S. Y. Jeong, L. L. Xu, C. H. Ryu, A. Kumar, S. Do Hong, D. H. Jeon, J. Y. Cho, J. H. Ahn, Y. H. Joo, I. W. Jeong, W. S. Hwang, T. H. Sung, Wearable Shoe-Mounted Piezoelectric Energy Harvester for a Self-Powered Wireless Communication System. *Energies* **15**, 237 (2021).
81. T.-C. Hou, Y. Yang, H. Zhang, J. Chen, L.-J. Chen, Z. Lin Wang, Triboelectric nanogenerator built inside shoe insole for harvesting walking energy. *Nano Energy* **2**, 856–862 (2013).
82. K. Zhang, X. Wang, Y. Yang, Z. L. Wang, Hybridized Electromagnetic–Triboelectric Nanogenerator for Scavenging Biomechanical Energy for Sustainably Powering Wearable Electronics. *ACS Nano* **9**, 3521–3529 (2015).
83. T. Huang, C. Wang, H. Yu, H. Wang, Q. Zhang, M. Zhu, Human walking-driven wearable all-fiber triboelectric nanogenerator containing electrospun polyvinylidene fluoride piezoelectric nanofibers. *Nano Energy* **14**, 226–235 (2015).
84. R. I. Haque, P.-A. Farine, D. Briand, Fully casted soft power generating triboelectric shoe insole. *J. Phys. Conf. Ser.* **773**, 012097 (2016).
85. R. I. Haque, P.-A. Farine, D. Briand, Soft triboelectric generators by use of cost-effective elastomers and simple casting process. *Sensors Actuators A Phys.* **271**, 88–95 (2018).
86. Y. Yun, S. Jang, S. Cho, S. H. Lee, H. J. Hwang, D. Choi, Exo-shoe triboelectric nanogenerator: Toward high-performance wearable biomechanical energy harvester. *Nano Energy* **80**, 105525 (2021).
87. W. Yuan, C. Zhang, B. Zhang, X. Wei, O. Yang, Y. Liu, L. He, S. Cui, J. Wang, Z. L. Wang, Wearable, Breathable and Waterproof Triboelectric Nanogenerators for Harvesting Human Motion and Raindrop Energy. *Adv. Mater. Technol.* **7**, 2101139 (2022).
88. X. Wang, W. Tong, Y. Li, Z. Wang, Y. Chen, X. Zhang, X. Wang, Y. Zhang, Mica-based triboelectric nanogenerators for energy harvesting. *Appl. Clay Sci.* **215**, 106330 (2021).
89. X. Yao, A flexible triboelectric nanogenerator based on soft foam for rehabilitation monitor after foot surgery. *Mater. Technol.*, 1–7 (2021).
90. Y. Gao, Z. Li, B. Xu, M. Li, C. Jiang, X. Guan, Y. Yang, Scalable core–spun coating yarn-based triboelectric nanogenerators with hierarchical structure for wearable energy harvesting and sensing via continuous manufacturing. *Nano Energy* **91**, 106672 (2022).
91. D. W. Lee, D. G. Jeong, J. H. Kim, H. S. Kim, G. Murillo, G.-H. Lee, H.-C. Song, J. H. Jung, Polarization-controlled PVDF-based hybrid nanogenerator for an effective vibrational energy harvesting from human foot. *Nano Energy* **76**, 105066 (2020).

Acknowledgments

Scanning electron micrographs in Fig. 1 were obtained at the Shared Equipment Authority at Rice University. This material is based upon work supported by the National Science Foundation Graduate Research Fellowship Program under Grant No. 1842494. Any opinions, findings, and conclusions or recommendations expressed in this material are those of the authors and do not necessarily reflect the views of the National Science Foundation.

Funding:

United States Coast Guard Advanced Education Program (RAS)
Rice University Academy of Fellows Program (AR)
NASA Space Technology Graduate Research Opportunity Award 80NSSC21K1276 (MDB)
National Science Foundation Graduate Research Fellowship Grant No. 1842494 (BJ)
National GEM Consortium GEM Fellowship (MDB, VS)
National Defense Science and Engineering Graduate Fellowship (VS)

Author contributions:

Conceptualization: RAS, AR, VS, DJP
Data curation: RAS, AR, TY, DJP
Formal analysis: RAS, AR, DJP
Methodology: RAS, AR, TY, ZL, DJP
Investigation: RAS, AR, TY, ZL, MDB, BJ, VS, DJP
Visualization: RAS, AR, TY, ZL, DJP
Software: RAS, AR, DJP
Project administration: RAS, DJP
Validation: RAS, AR, DJP
Supervision: DJP
Writing—original draft: RAS, AR, DJP
Writing—review & editing: RAS, AR, TY, ZL, MDB, BJ, VS, DJP

Competing interests: Authors declare that they have no competing interests.

Data and materials availability: All data are available in the main text or the supplementary materials.

Figures and Tables

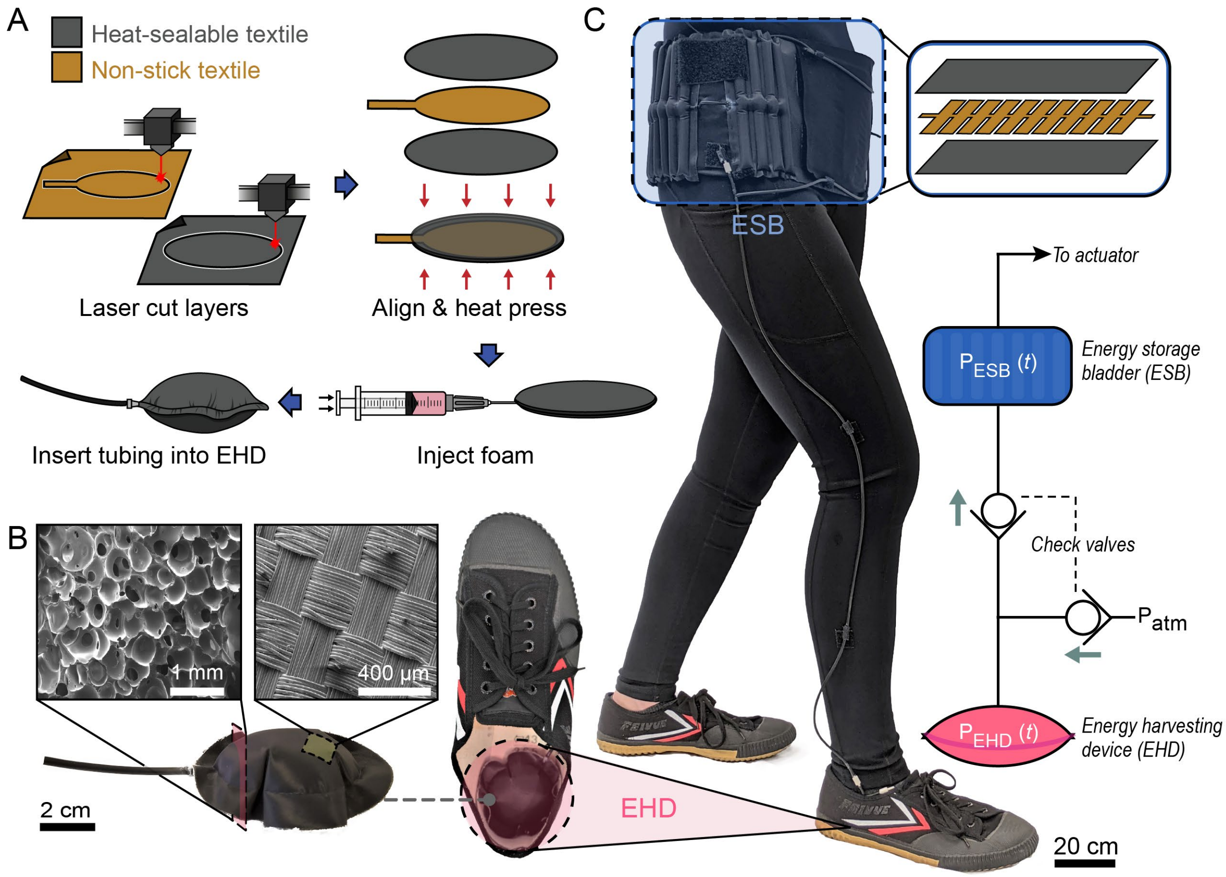

Fig. 1. Fabrication and donning of the textile-based energy harvesting system. (**A**) Fabricating the insole EHD from heat-sealable textile layers. (**B**) Scanning electron micrographs of EHD components: open-cell foam interior and textile exterior. (**C**) A user wearing the fully assembled system. The EHD is integrated into the insole of the right shoe, and the textile ESB is worn around the waist. Insets show the textile layers used to fabricate the ESB, and a schematic diagram of the pneumatic circuit linking the EHD and ESB.

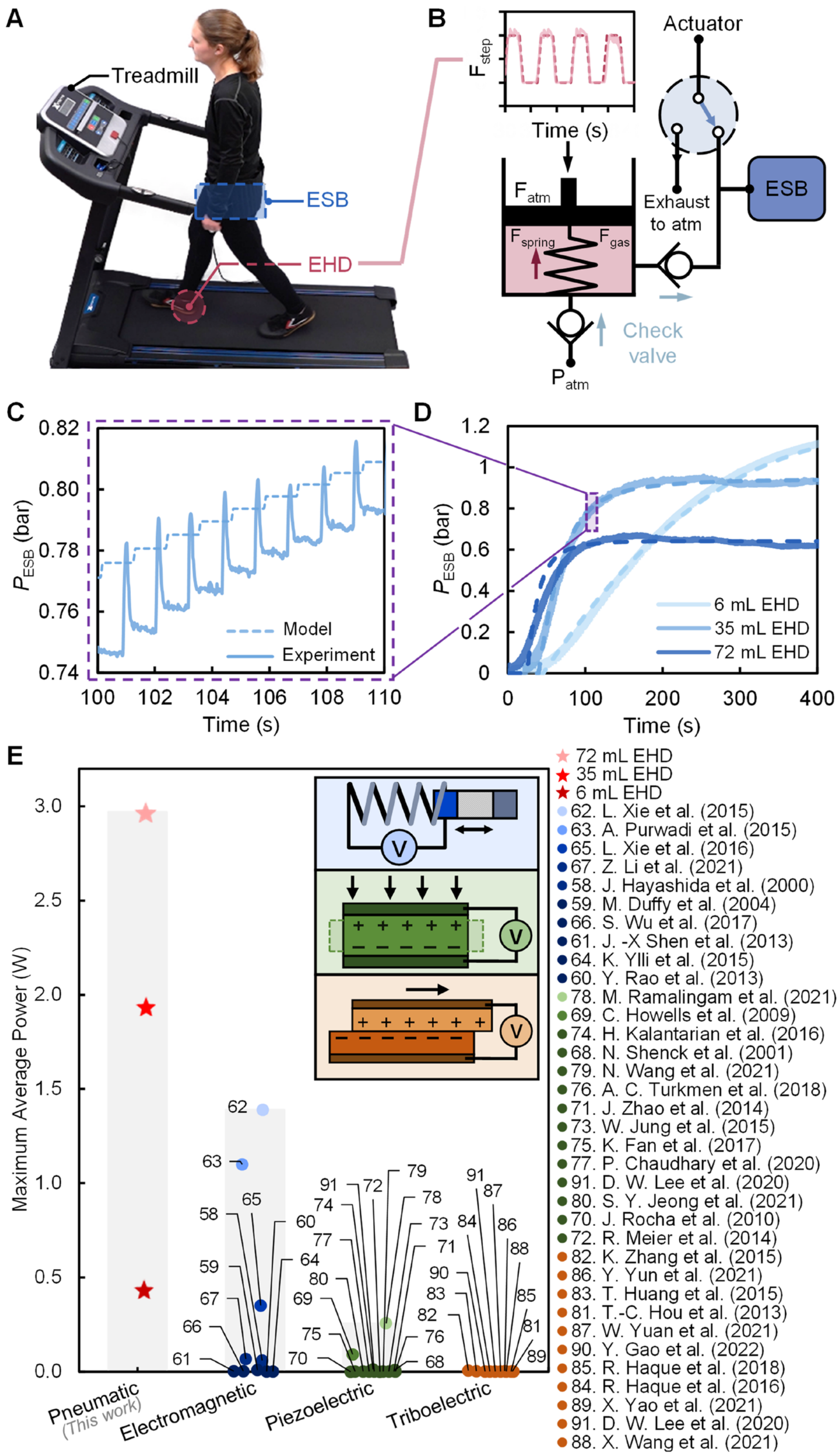

Fig. 2. Characterizing the performance of the energy harvesting system. (**A**) A user wearing the energy harvesting system walks on a treadmill during experimental measurements. (**B**) Schematic representation of the mechano-fluidic model used for performance evaluation and optimization. The inset shows the experimentally measured stepping force (solid curve) along with the matching trapezoidal waveform (dashed curve) used to model it. (**C**) Transient pressure traces predicted by the model (dashed curves) were validated against experimental measurements (solid curves). (**D**) Predicted and measured gas pressure inside the ESB for a 55 kg user walking at 3 mph. (**E**) Comparison of the maximum power output of the insole EHD with existing electromagnetic, piezoelectric, and triboelectric foot-strike energy harvesting systems.

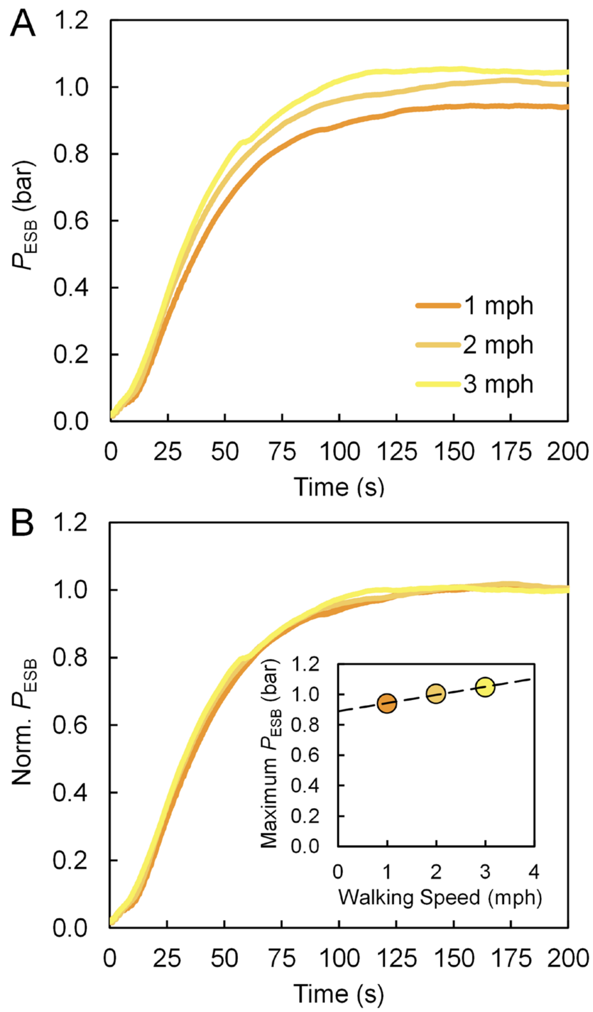

Fig. 3. Effect of walking speed on energy harvesting performance. (**A**) Evolution of ESB pressure with time for the 35 mL EHD and for a 72 kg human user walking at different speeds. Each curve represents transient pressure data smoothed over two step cycles and averaged over three replicate measurements. (**B**) The pressure traces in (A) collapse when normalized by the maximum ESB pressure, suggesting that the fill rate is independent of walking speed. The inset shows a small increase in the final gas pressure in the ESB at faster walking speeds.

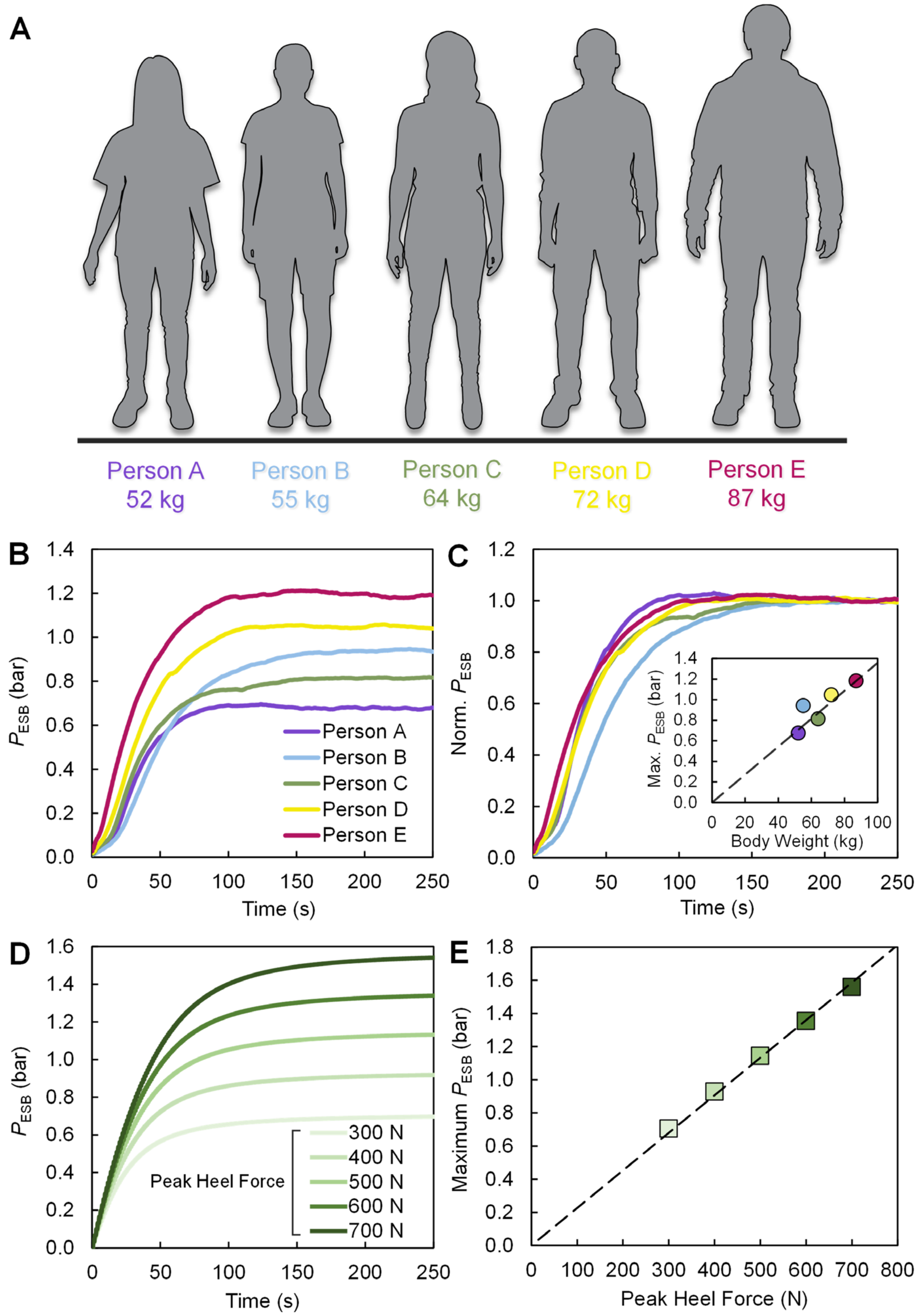

Fig. 4. Evaluating system performance for users of different bodyweights. (**A**) The cohort of test users representing a range of bodyweights, leg lengths, and foot sizes. (**B**) ESB pressure recorded as a function of time for the 35 mL EHD and for the five users all walking at 3 mph. Raw pressure data were smoothed over two step cycles and then averaged over three replicates. (**C**) Pressure traces in (B) normalized by the maximum ESB pressure show no significant variation in fill time between users. The inset indicates that the maximum ESB pressure increases proportionally with the user's bodyweight. (**D**) Transient responses of the mechano-fluidic model from a parametric sweep of the amplitude of stepping force, simulating users of different weights. (**E**) The final ESB pressure in (D) increases proprtionally with the peak heel force exerted on the EHD.

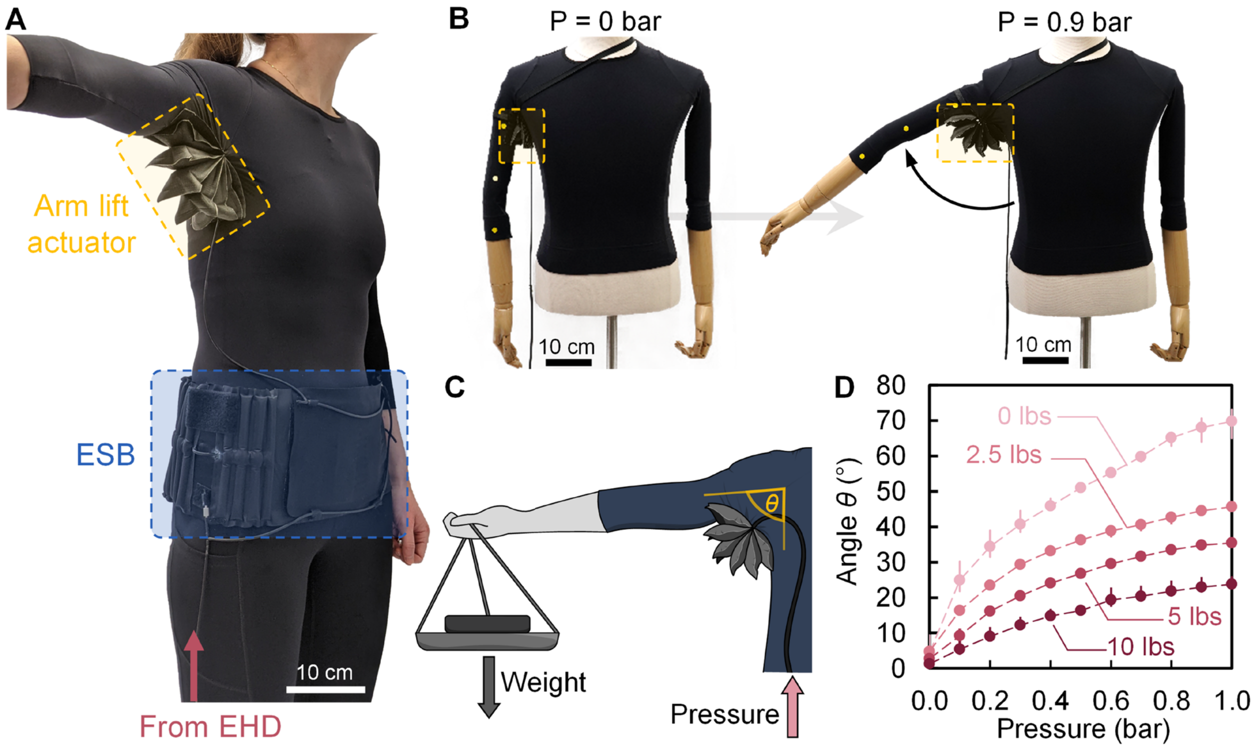

Fig. 5. The pneumatic arm-lift assistive actuator. (**A**) The actuator mounted on the user's garment beneath the shoulder, shown in an actuated state after pressurization with compressed air generated by the user. (**B**) When pressurized, the actuator imparts a lifting torque on the shoulder joint of a mannequin; the mannequin was used to preclude any influence of muscular effort when testing on a human user. (**C**) Schematic representation of the experimental setup used to characterize the lifting torque. (**D**) The angular displacement of the arm produced by the actuator as a function of the input pressure and the weight suspended from the arm. Data markers denote averaged measurements, and the error bars indicate the range of observed angles across three replicates.

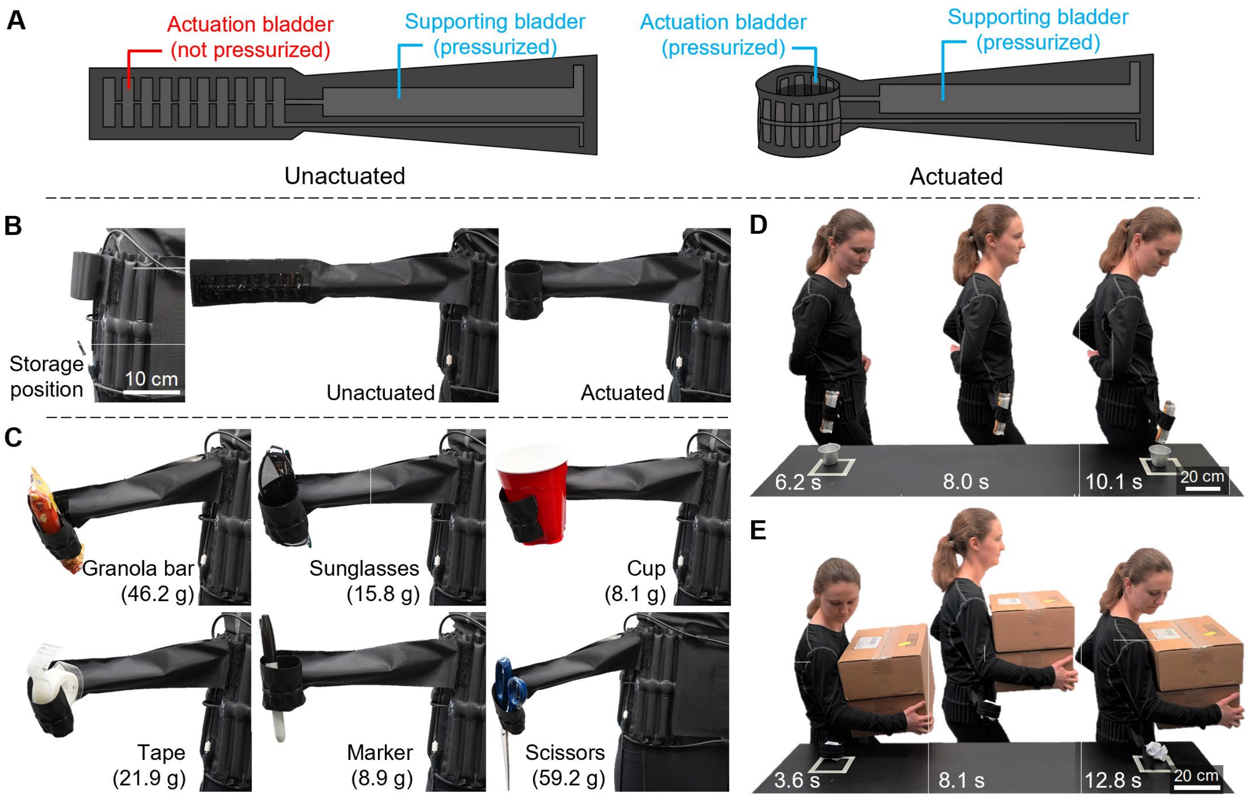

Fig. 6. The supernumerary robotic arm powered by the energy harvesting system. (**A**) Schematic diagram of the dual-bladder system that lends mechanical strength and enables gripper actuation. (**B**) The third arm in the storage, deployed (unactuated), and actuated configurations. (**C**) The third arm gripping objects of various shapes, weights, and surface textures. (**D**) A time-lapse sequence of the user employing the third arm to pick up, transport, and deliver a 43 g granola bar. (**E**) The third arm used to pick up and transport a crumpled piece of paper while the user's arms are full.

Supplementary Materials

Supplementary Text
Figs. S1–S12
Tables S1–S7
References *58–91*
Movies S1–S3
Data S1 and S2

Science Advances
AAAS

Supplementary Materials for

A Wearable Textile-Based Pneumatic Energy Harvesting System for Assistive Robotics

Rachel A. Shveda, Anoop Rajappan, Te Faye Yap, Zhen Liu, Marquise D. Bell, Barclay Jumet, Vanessa Sanchez, Daniel J. Preston*

*Corresponding author. Email: djp@rice.edu

This PDF file includes:

Supplementary Text
Figs. S1 to S12
Tables S1 to S7
References (*58* to *91*)

Other Supplementary Materials for this manuscript include the following:

Movies S1 to S3
Data S1 and S2

Supplementary Text

Mechano-fluidic model for the textile-based energy harvesting system

Ideal gas law. The ideal gas law is used to model air temperature and pressure inside the insole pouch and the wearable tank:

$$PV = mRT \tag{S1}$$

Here P is the pressure, V is the volume, m is the mass, R is the specific gas constant for air, and T is the absolute temperature. The gas pressure within the EHD, $P_{EHD}(t)$, and inside the wearable ESB, $P_{ESB}(t)$, are both initially equal to atmospheric pressure. The mass of air inside the EHD, $m_{EHD}(t)$, is calculated as:

$$m_{EHD}(t) = \frac{P_{EHD}(t)V_{EHD}}{RT_S} \tag{S2}$$

where V_{EHD} is the volume of the EHD, and T_S is the temperature inside the user's shoe.

Internal gas volumes of EHDs were determined experimentally using a universal testing machine (68SC-2, Instron). The EHD was compressed between the flat platens of the Instron, with the outlet connected to a long clear tube open at the other end to atmosphere. A small liquid plug (of approximately 0.2 mL of dyed water) was introduced into the clear tubing at the end closest to the EHD outlet. The movement of the plug inside the tube was tracked as the EHD was slowly compressed, and the volume of air expelled from the EHD was inferred as the product of the displacement of the plug and the known cross-sectional area of the tube. The changing volume of the EHD with compression is approximated using a piecewise quadratic function of the form:

$$V_{EHD}(x) = \begin{cases} A - Bx - Cx^2 & 0 \le x \le x_m \\ 0 & x \ge x_m \text{ (where } A - Bx_m - C{x_m}^2 = 0) \end{cases} \tag{S3}$$

where x is the distance by which the EHD is compressed. The coefficients of the polynomial were obtained by least-squares regression to the experimentally measured volume data (Fig. S4). The compression at zero volume, x_m, is the compression at which the gas volume inside the pouch is assumed to be zero; this quantity was set equal to the displacement at which the reaction force from the EHD (as measured on the Instron) began rising rapidly, indicating the "bottoming-out" of the EHD.

The average shoe temperature T_S was measured using a thermocouple taped to the insole of the user's shoe during experiments. During the compression phase, air inside the EHD heats up because of fast, near-adiabatic compression by the falling foot during each step. It then cools down over the remainder of the stepping cycle because of heat loss to the environment, and by mixing with the cool air drawn in during the intake phase. The air temperature thus rises and falls cyclically as stepping progresses. For simplicity, this variation (which was observed to have a magnitude of less than 5 K) is neglected in the model, and air inside the EHD is assumed to be at a steady, "effective" temperature. This effective temperature was measured during stepping experiments and found to be T_S = 296 K.

The wearable ESB is modeled as a flexible but inelastic bladder that is partly inflated at the start of the experiment. The air inside the ESB is assumed to always be at room temperature. The degree of inflation at $t = 0$ is set by an adjustable parameter, f_{ESB}, which controls the initial mass of air inside the ESB. As air is pumped in by the EHD, the pressure inside the ESB is assumed to remain atmospheric until full inflation is reached (i.e., while the storage space within the ESB transitions from flat chambers to a series of expanded flexible textile cylinders). The mass of air at full inflation, $m_{ESB,c}$, is calculated as:

$$m_{ESB,c} = \frac{P_a V_{ESB}}{RT_a} \tag{S4}$$

where P_a is the atmospheric pressure, V_{ESB} is volume of the ESB when fully inflated, and T_a is the ambient temperature. Once inflated, the ESB is assumed to remain at its maximum volume, which we estimated from the overall geometry of its chambers to be 744 mL. The initial mass of air in the ESB at the start of the experiment is given by:

$$m_{ESB}(0) = f_{ESB} m_{ESB,c} \tag{S5}$$

A loop, implemented in MATLAB, steps through time at small intervals of dt seconds—with the stepping force $F_{step}(t)$ applied to the EHD at a certain rate—to compute the internal pressures in the system components as the user walks for a set period (Data S1).

Force balance on the EHD. At any given timestep in the loop, four forces act on the top wall of the EHD, as shown in Fig. 2B. We perform a force balance on the EHD to determine the distance of compression, x, given by:

$$F_{step} + F_{atm}(x) - F_{spring}(x) - F_{gas}(x, m_{EHD}) = 0. \tag{S6}$$

Here F_{step} is the instantaneous force exerted by the user's foot, F_{atm} is the force from atmospheric pressure, F_{spring} is the restoring force from the foam inside the EHD, and F_{gas} is the force from internal gas pressure. The force from atmospheric pressure is given by:

$$F_{atm} = P_a A \tag{S7}$$

where A is the effective contact area of the EHD, assumed equal to the projected area of its lenticular pouch. To find this area, the geometry of the pouch is modeled as two spherical caps joined at the seam, each with a curved surface area that remains constant with compression. Vernier calipers were used to measure the projected radii, a_{EHD}, and heights, h_{EHD}, of the undeformed EHD pouches. We then set:

$$\pi \left[a_{EHD}^2 + \left(\frac{h_{EHD}}{2} \right)^2 \right] = \pi \left[a^2(x) + \left(\frac{h_{EHD} - x}{2} \right)^2 \right] \tag{S8}$$

where $a(x)$ denotes the projected radius of the deformed EHD when compressed through by a distance x. The contact area is then approximated as:

$$A(x) = \pi a^2(x) \tag{S9}$$

The force from gas pressure is calculated as:

$$F_{gas} = \frac{m_{EHD} R T_S}{V_{EHD}(x)} A(x) \tag{S10}$$

where the internal volume of the EHD, $V_{EHD}(x)$, was modeled using the quadratic polynomial in Eq. S3 above.

Stepping force. A force sensing resistor (FSR 406, Interlink Electronics) was used to monitor the stepping force exerted by the user's foot on the EHD when walking on a treadmill

(TR150, Xterra Fitness) at a constant pace. Sample measurements for the 35 mL EHD prototype are shown in Fig. S5A. Transient data was collected by means of an analog voltage acquisition device (USB-6211, National Instruments) in conjunction with the voltage divider circuit shown in Fig. S5B; the force sensor was connected in series with a 47.5 Ω resistor across a 5 V DC source. The data was converted to resistance, and then to force, using the sensor's response curve (Fig. S5C).

The stepping force on the EHD was idealized as a trapezoidal waveform in the numerical model. The force amplitude was estimated by matching peak pressures attained inside the EHD during walking and under simulated compression using a universal testing machine (86SC-2, Instron). First, a pressure sensor was connected to the EHD outlet and the gas pressure inside the EHD was recorded with the user walking on the treadmill. Then, the EHD was placed between the platens of the Instron with the outlet connected to a digital pressure gauge. The force exerted by the platen was monitored during rapid compression of the EHD, and the amplitude of the trapezoidal waveform was set equal to the peak force for which the maximum gas pressure attained inside the EHD matched that recorded during walking on the treadmill. The time period, duty cycle, and the slope of the rising and falling edges of the trapezoidal function were matched to the experimental waveform measured by the insole force sensing resistor as the user walked on the treadmill (Fig. S5A).

Restoring force from the foam. The Neo-Hookean model for hyperelastic solids is a non-linear elastic model commonly used to represent the large strain response of elastomers, rubbers, and other soft flexible materials. The restoring force exerted by the foam inside the EHD was modeled using a Neo-Hookean-type force function given by:

$$F_{spring}(x) = C\left(\frac{1}{\lambda^2} - \lambda\right) \tag{S11}$$

where λ is the stretch ratio,

$$\lambda = \frac{h_{EHD} - x}{h_{EHD}} \tag{S12}$$

and C is a constant pre-factor obtained by regression to the force vs compression data obtained from measurements on the universal testing machine (86SC-2, Instron). During this test, the EHD was placed between the platens of the machine with its outlet open to the atmosphere, and gradually compressed at a rate of 0.5 mm/s. The resulting force vs displacement curves for all three EHD prototypes, along with the corresponding Neo-Hookean fits, are shown in Fig. S6.

Time-stepping loop. At each timestep, MATLAB's inbuilt non-linear iterative root finding algorithm, fzero, is used to solve Eq. S6 to determine the equilibrium compression $x(t)$ of the EHD; the compression $x(t-dt)$ at the previous time step is used as the initial guess for the solver. Next, the gas pressure inside the EHD is calculated:

$$P_{EHD}(t) = \frac{m_{EHD}(t)RT_S}{V_{EHD}[x(t)]} \tag{S13}$$

We then check for mass flow out of the EHD to the ESB or into the EHD through the intake valve. If $P_{EHD}(t) > P_{ESB}(t)$ then air flows from the EHD to the ESB; here $P_{ESB}(t)$ is the air pressure inside the ESB. The flow rate of air into the ESB, Q_{ESB}, is calculated as:

$$Q_{ESB} = \frac{P_{EHD} - P_{ESB}}{r_o} \tag{S14}$$

where r_o is the fluidic resistance of the tube connecting the EHD to the ESB. Here, we assume that the pressure drop across tubes is proportional to the flow rate,

$$\Delta P = rQ \tag{S15}$$

which is true when the flow inside the tubes is laminar. The resistance of check valves and other connectors is assumed negligible, as corroborated by experimental measurements. The flow resistance of the outlet tube connecting the EHD to the ESB was estimated experimentally by measuring the pressure drop across the tube using a pressure gauge while imposing known constant flow rates of air through the tube using a syringe pump. The mass of air transferred to the ESB, dm_{ESB}, is calculated as:

$$dm_{ESB} = \frac{P_{EHD} Q_{ESB} dt}{RT_S} \tag{S16}$$

with the restriction that the mass of air transferred cannot exceed the total mass of air available inside the EHD, $dm_{ESB} \leq m_{EHD}(t)$.

If $P_{EHD}(t) < P_a$ then ambient air flows through the intake valve into the EHD. Flow rate into the EHD from the atmosphere, Q_a, is calculated as:

$$Q_a = \frac{P_a - P_p}{r_i} \tag{S17}$$

where r_i is the fluidic resistance of the intake tube, also determined experimentally using a syringe pump as described above. Since the inlet resistance is negligibly small, the pressure inside the EHD remains near atmospheric during most of the reinflation phase. The mass of air transferred into the EHD from atmosphere, dm_a, is then given by:

$$dm_a = \frac{P_a Q_a dt}{RT_a}, \tag{S18}$$

with the constraint that the mass of air transferred cannot exceed the mass of air required to refill the EHD to ambient pressure; this maximum value is given by:

$$dm_{max} = \frac{P_a V_{EHD}[x(t)]}{RT_S} - m_{EHD}(t) \tag{S19}$$

where $m_{EHD}(t)$ is the mass of air currently inside the EHD.

Lastly, the mass of air inside the EHD and the ESB are updated. The mass inside the ESB becomes:

$$m_{ESB}(t + dt) = m_{ESB}(t) + dm_{ESB} \tag{S20}$$

If $m_{ESB} > m_{ESB,c}$, then the ESB is fully inflated, and its internal gas pressure is given by the ideal gas law:

$$P_{ESB} = \frac{m_{ESB} RT_a}{V_{ESB}}; \tag{S21}$$

otherwise, the ESB is only partly inflated, and the pressure is set equal to the atmospheric pressure. The mass inside the EHD is also updated according to:

$$m_{EHD}(t + dt) = m_{EHD}(t) - dm_{ESB} + dm_a \tag{S22}$$

before the next iteration of the loop.

Model predictions for the 6 mL, 35 mL, and 72 mL EHD prototypes, in conjunction with the 744 mL ESB, are shown in Fig. S9. The smallest (6 mL) EHD had the slowest rate of fill but achieved the highest ESB pressure, equal to 1.2 bar. The largest (72 mL) EHD had the fastest rate of fill but achieved the lowest ESB pressure of 0.6 bar. The 35 mL EHD had a rate of fill intermediate to those of the 6 mL and 72 mL EHDs, and achieved an ESB pressure of 0.9 bar.

Power output and efficiency. We define the energy conversion efficiency of our system as:

$$\eta = \frac{\text{Energy stored in the ESB when full}}{\text{Total mechanical work done by the foot}} \times 100\% \tag{S23}$$

First, stored energy in the ESB is calculated as the reversible work of expansion (against the atmosphere) of the pressurized air contained in the ESB:

$$W = m_{ESB} R T_a \ln\left(\frac{P_{ESB}}{P_a}\right) \tag{S24}$$

The stored energy is shown as a function of time in Fig. S7A. The power output of the EHD for step n was computed as the rate of increase in stored energy averaged over one stepping cycle of duration T:

$$\dot{W} = \frac{W(nT + T) - W(nT)}{T}. \tag{S25}$$

The power output of the EHD is shown as a function of time in Fig. S7B, and as a function of ESB pressure in Fig. S8. For computing the efficiency, we compare the stored energy and the input work until "full inflation" of the ESB, which we take to be the point when the ESB pressure reaches 99% of its final value:

$$P_{ESB}(t_{full}) - P_a = 0.99[P_{ESB}(\infty) - P_a] \tag{S26}$$

This full inflation point is marked in Fig. S9 for all three EHD prototypes. The total work done by the foot in compressing the EHD is calculated by integrating the instantaneous downward stepping force, $F_{step}(t)$, with respect to the resulting compression dx of the EHD wall; any negative work done by the EHD on the foot during the intake phase is discarded in computing this total work, yielding a conservative estimate.

A brief note on the durability of textile-based devices

A crucial consideration for wearable devices is their durability under the rigors of everyday use. Our choice of structural materials—namely, nylon taffeta fabric and polyurethane foam—for building the EHD and ESB make these devices capable of withstanding rough handling and cyclic loading anticipated during routine service. Over the course of this study, our EHD and ESB prototypes have been subjected to several hours of cumulative tests involving five users of various bodyweights (52–87 kg) walking on a treadmill at different speeds (1–3 mph, or 1.6–4.8 km/h).

For instance, the 35 mL EHD has endured more than 200 minutes of cumulative walking tests, equivalent to a total distance of over 9 miles (14.5 km). Similarly, the ESB has undergone over 100 pressurization and depressurization cycles without structural failure or leaks. To further verify the durability of our device, we built a mechanical test rig that simulates the repetitive compression of the EHD by the user's foot during walking, with which we subjected the 35 mL EHD to an additional 200,000 loading-unloading cycles at a simulated footfall frequency of 1 Hz. Neither component sustained any discernible structural damage or performance deterioration because of these extensive tests, indicating a promising outlook for the long-term reliability of our devices. However, a future systematic investigation of their durability under accelerated wear conditions would be helpful in proving their suitability for prolonged use.

As a step in this direction, we tested the durability of our devices under machine washing; specifically, we subjected the 35 mL EHD to five wash cycles with laundry detergent (Tide Free and Gentle, Procter & Gamble) inside a household washing machine (model WF45R6100AW/US, Samsung Electronics Co. Ltd.) and tested its performance afterwards. The data are shown in Fig. S12 for a 52 kg user walking on the treadmill at 3 mph. Comparison of ESB pressure traces recorded before and after washing the EHD show no significant changes in system performance, neglecting slight fluctuations on account of natural variations in the user's gait.

As with the EHD and ESB prototypes, the two assistive actuators—the arm-lift and the supernumerary arm—have both been subjected to multiple rounds of actuation over the course of this study; for instance, the arm-lift actuator underwent more than 150 pressurization events, with suspended loads of up to 15 lbs (6.8 kg), without incurring any discernible structural damage or loss of function (Fig. 5D). We also tested the arm-lift afterwards for an additional 1000 actuation cycles using an automated pneumatic test rig, and again observed no damage or deterioration. We did not undertake a more detailed characterization of our assistive actuators because they were intended mainly as practical demonstrations of the capabilities of our energy harvesting system—the EHD and ESB—which forms the core focus of our work. A variety of assistive actuators, similar in design and function to our arm-lift device and supernumerary arm, have been extensively reviewed and characterized in the extant literature; in principle, any of these actuators powered using compressed air may be coupled to our energy harvesting system with minimal or no modification.

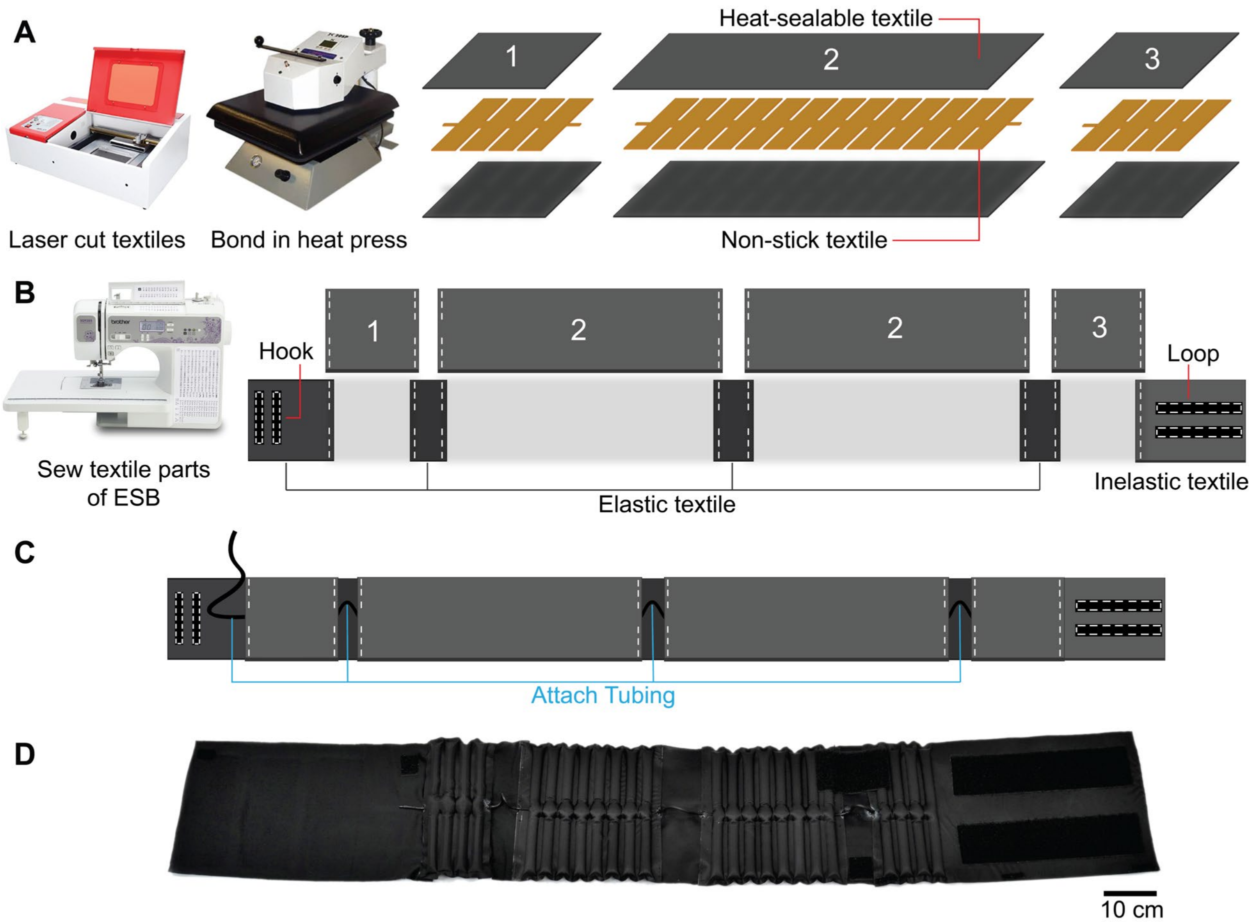

Fig. S1. Fabrication of the wearable ESB. (A) Schematic of textile layers cut using a laser cutter and arrangement for heat sealing. (B) Sewing pattern for addition of elastic textile, inelastic textile, and hook and loop fasteners. (C) Schematic of final wearable ESB after attachment of pneumatic lines. (D) Photograph of the completed prototype of the wearable ESB.

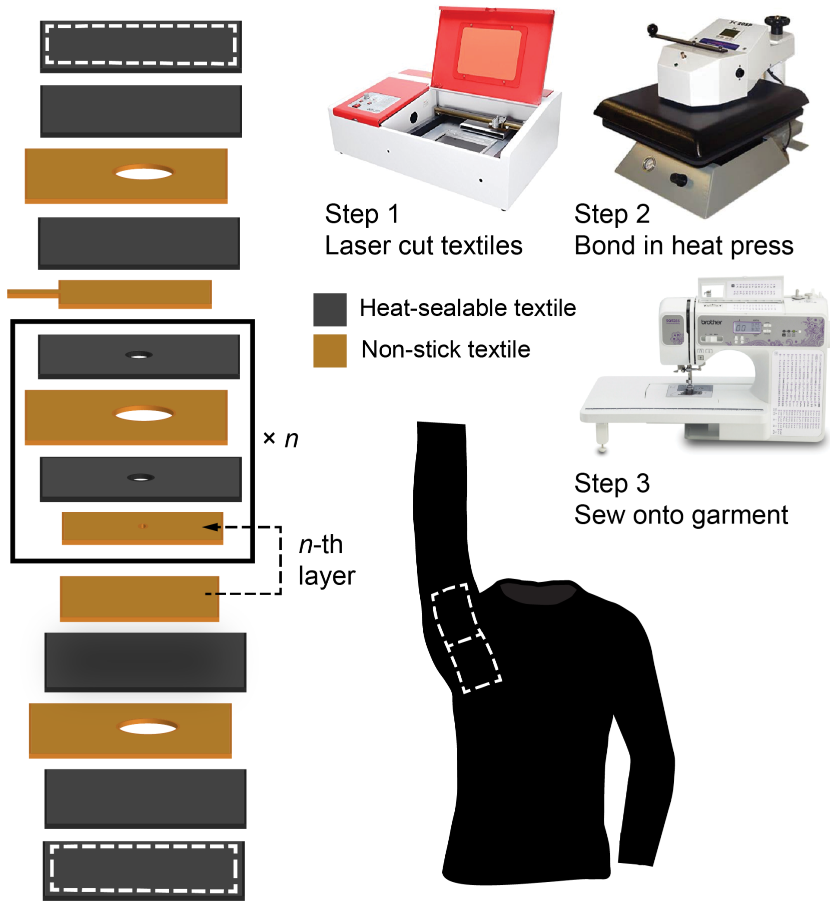

Fig. S2. Fabrication of the arm-lift assistive device. The schematic diagram on the left shows the textile layers of the arm-lift actuator and their arrangement for bonding. The sketch on the bottom right depicts the sewing pattern for attachment to the armpit of a compression shirt.

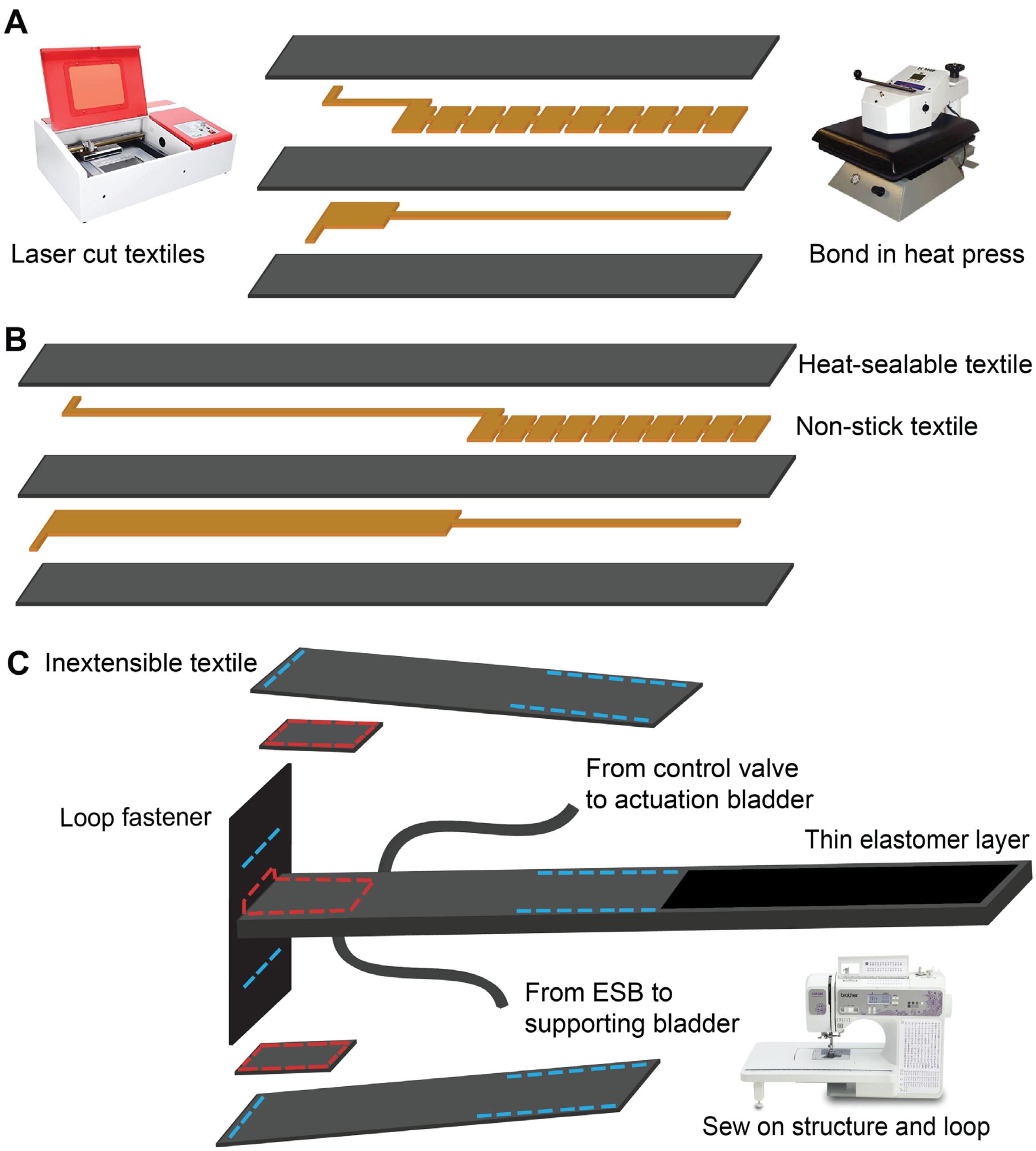

Fig. S3. Fabrication of the supernumerary robotic arm. Schematic diagrams of textile layers and their arrangement for bonding for (A) the "short" and (B) the "long" supernumerary robotic arms. (C) Sewing patterns for inelastic-textile-based structural additions and loop fastener for ESB mounting.

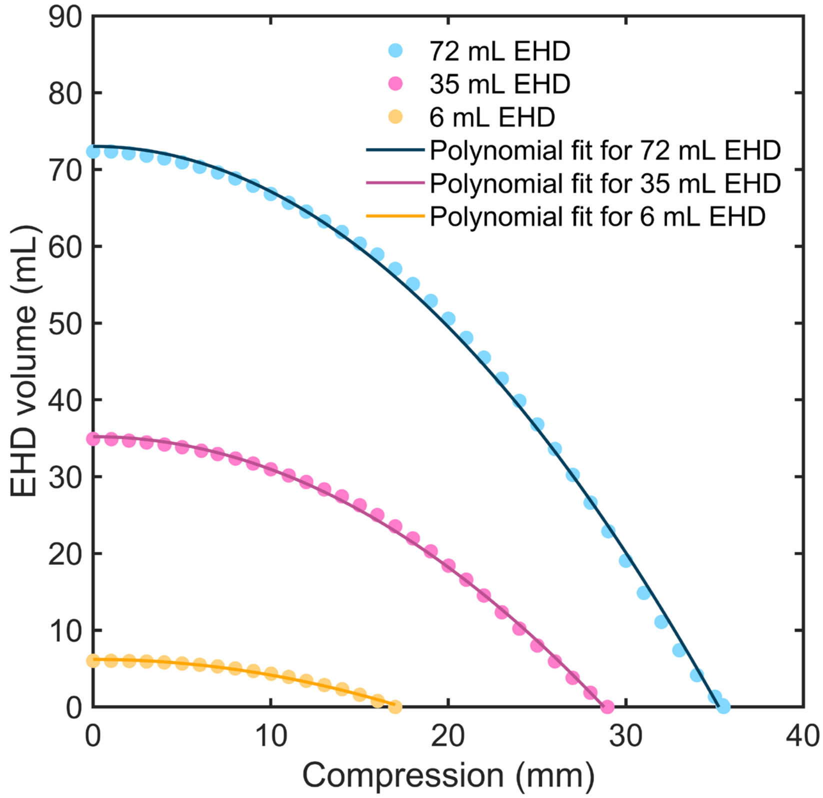

Fig. S4. Experimental measurements of the internal gas volume of insole EHDs as a function of compression. The solid curves denote polynomial fits to the experimental data of the form $V(x) = A - Bx - Cx^2$, where $V(x)$ is the volume in mL and x is the compression in mm. The fit coefficients are given by A = 73.00, $B = 2.581 \times 10^{-11}$, and C = 0.05881 for the 72 mL EHD; A = 35.20, $B = 1.774 \times 10^{-11}$, and C = 0.04253 for the 35 mL EHD; and A = 6.199, $B = 1.4600 \times 10^{-11}$, and C = 0.02043 for the 6 mL EHD.

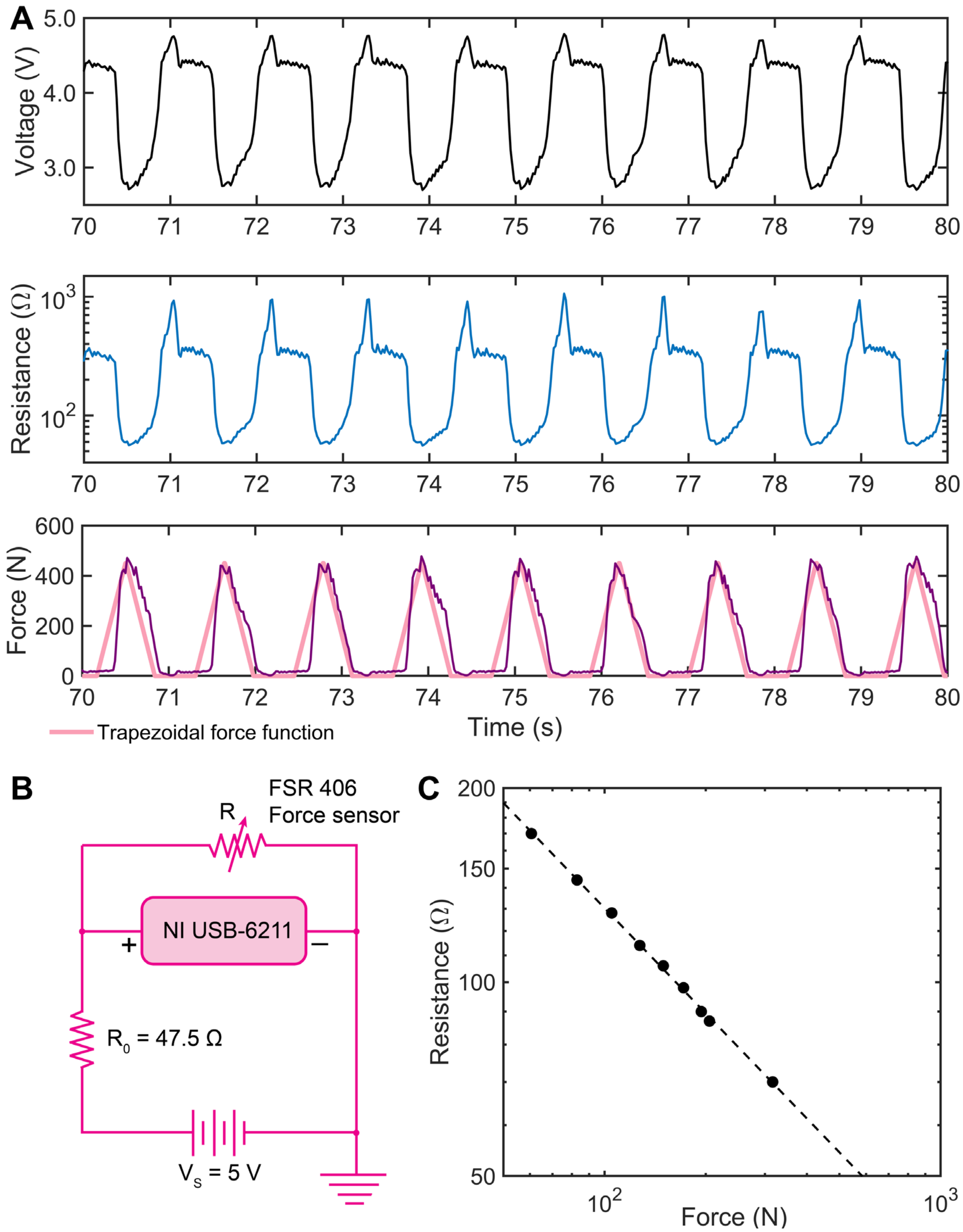

Fig. S5. Experimental characterization of stepping force. (A) Stepping force measured as a function of time for the 35 mL EHD and for a walking speed of 3 mph. The measured output voltage from the sensor was converted first to resistance and then to force using a calibration curve. (B) Schematic of the voltage divider circuit used to monitor changes in sensor resistance. (C) Resistance-to-force calibration data for the FSR 406 obtained by applying a range of known weights and measuring sensor resistance.

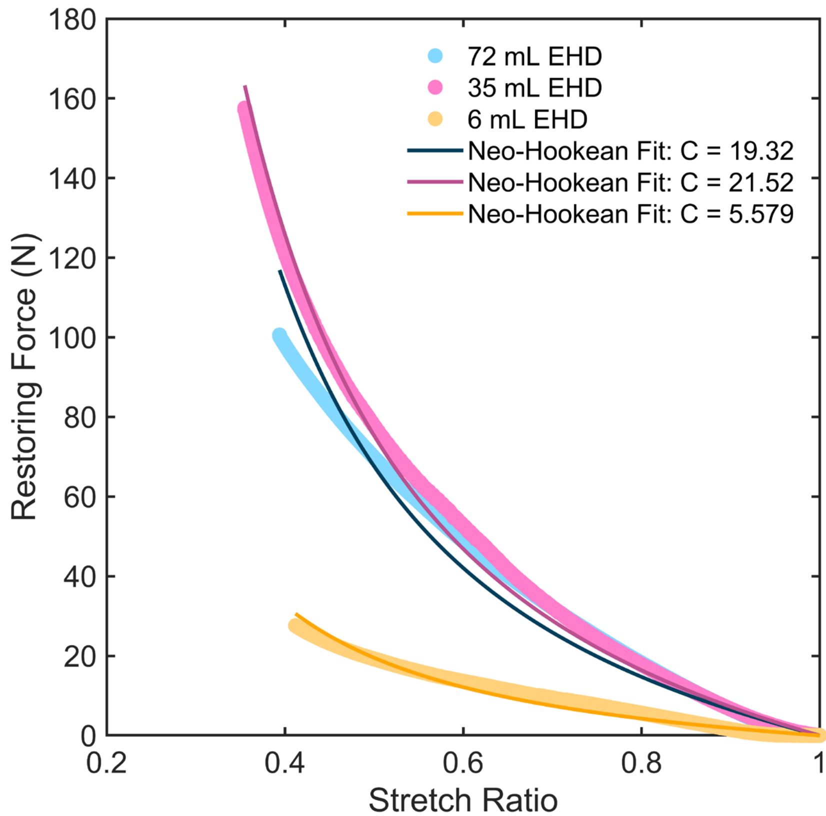

Fig. S6. Experimental measurement of the restoring force from the foam inside the EHD pouch. Force measurements were acquired by compressing each of the three EHD prototypes on a universal testing machine (Instron 68SC-2).

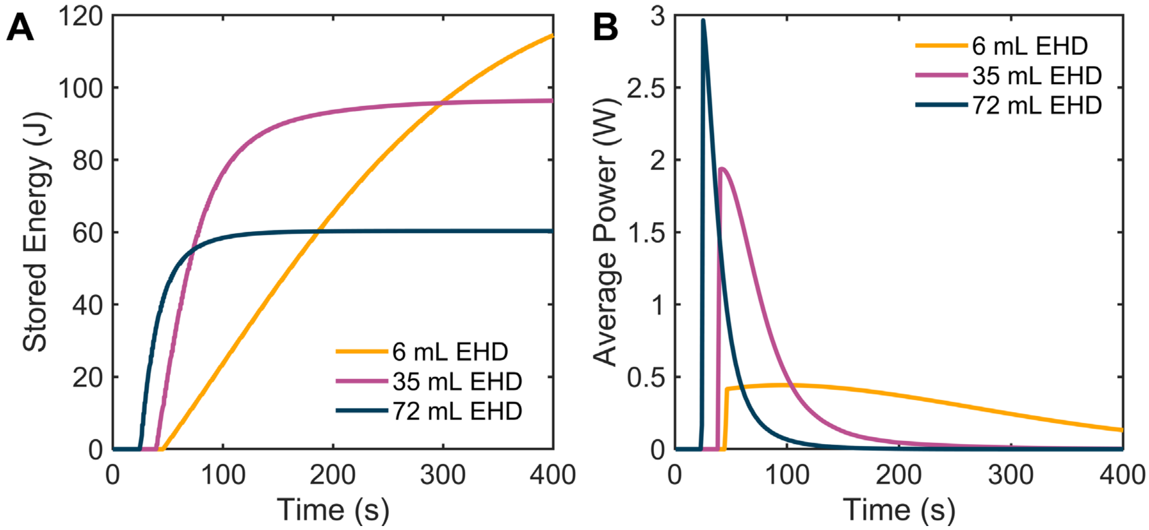

Fig. S7. Performance of the textile-based energy harvesting system. (A) Stored energy in the ESB as a function of time with the user walking at 3 mph. (B) Power output from the EHD averaged over each stepping cycle.

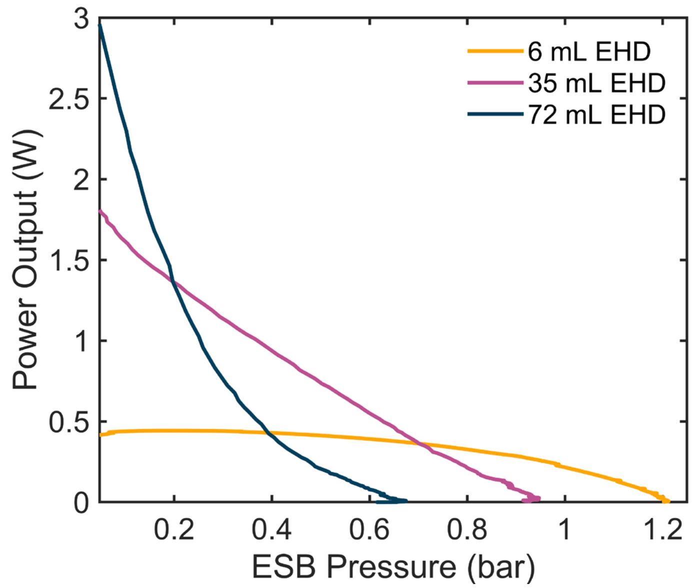

Fig. S8. Variation in output power as a function of ESB pressure for the 6 mL, 35 mL, and 72 mL EHD prototypes. This plot indicates the steady power output that may be drawn from the system by a balanced load at a given pressure.

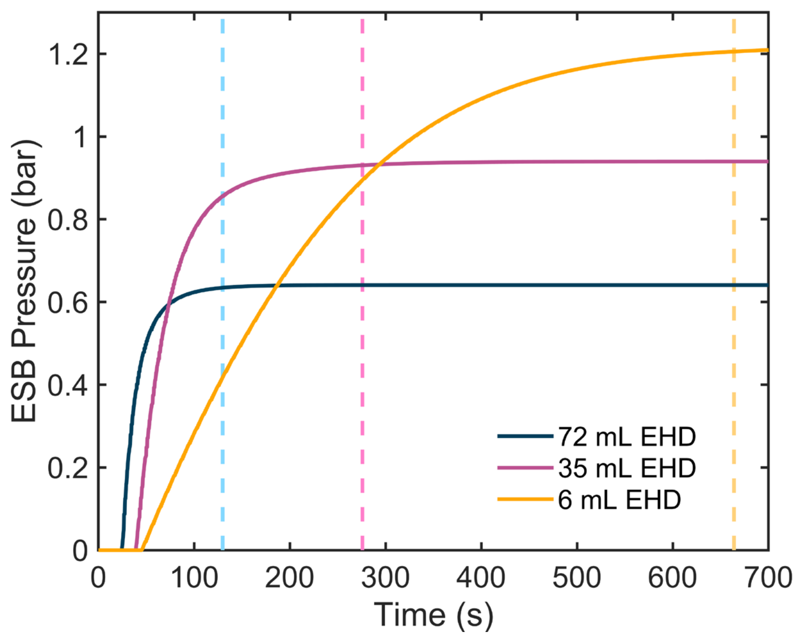

Fig. S9. Time to full ESB inflation. ESB pressure as a function of time based on the mechano-fluidic model for the 6 mL, 35 mL, and 72 mL EHD prototypes. The vertical dashed lines denote the point of "full inflation" of the ESB (when gas pressure reaches 99% of the final steady-state value), used in the computation of the conversion efficiency.

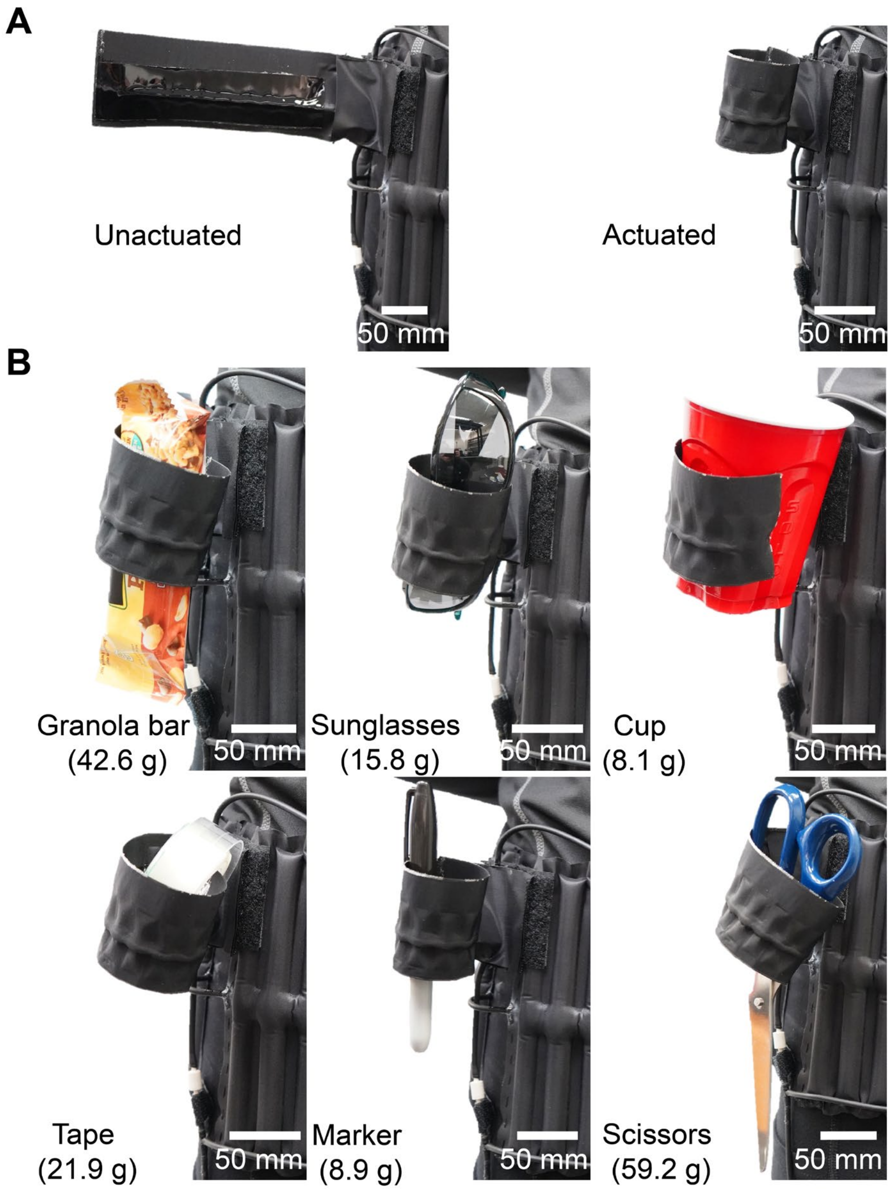

Fig. S10. Demonstration of the short supernumerary arm powered by the textile-based energy harvesting system. (A) The short arm in the unactuated and actuated configurations. (B) The actuated arm grasping objects of various shapes and weights: a granola bar (42.6 g), a pair of sunglasses (15.8 g), a cup (8.1 g), a tape roll (21.9 g), a marker pen (8.9 g), and a pair of scissors (59.2 g). The long version of the supernumerary arm is shown in the main text.

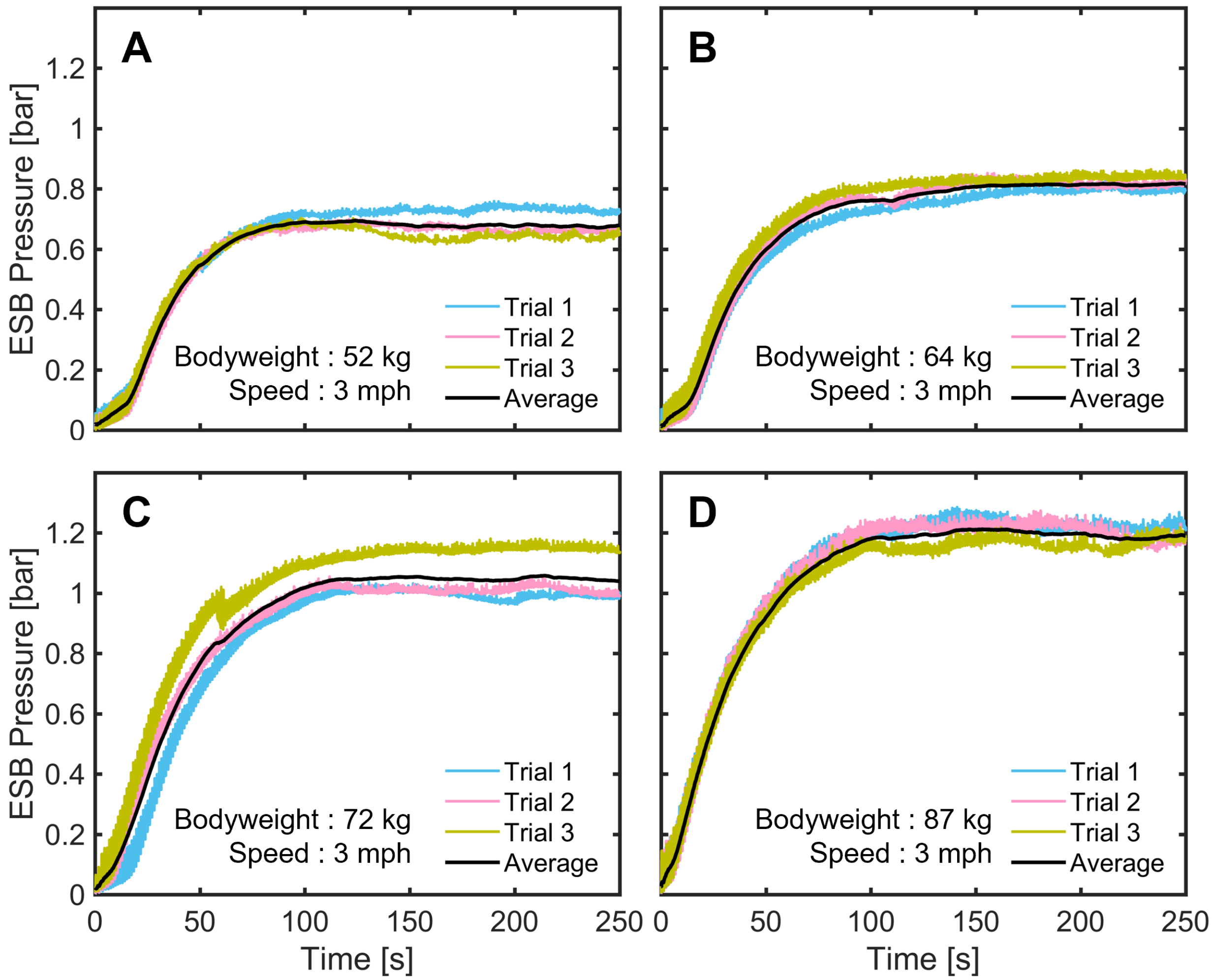

Fig. S11. Characterization of energy harvesting performance for multiple users. (A–D) ESB pressure as a function of time for the 35 mL EHD, and for users of different body weights, all walking at 3 mph. Included in each plot are the raw pressure data for 3 replicate tests, and the averaged pressure curve smoothed over two step cycles for each user.

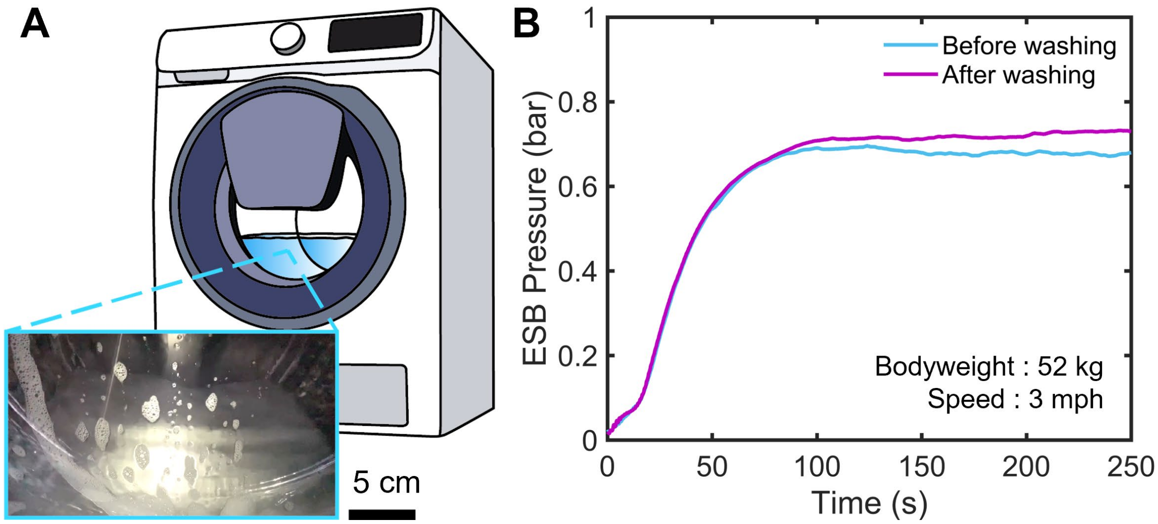

Fig. S12. Durability of the textile EHD under machine washing. (A) The 35 mL EHD was machine washed five times with laundry detergent inside a front-load washing machine. (B) ESB pressure traces recorded both before and after washing (for a 52 kg user walking at 3 mph) showed no deterioration in pumping performance.

Table S1. Material cost for fabricating insole EHDs.

	6 mL	35 mL	72 mL
Heat-sealable textile (\$14.95/1.67 yd^2)	\$0.16	\$0.55	\$0.85
Non-stick textile (\$13.95/1.67 yd^2)	\$0.04	\$0.15	\$0.28
Polyurethane foam (\$27.78/pint)	\$0.13	\$0.79	\$1.61
Soft tubing (\$0.42/ft)	\$0.11	\$0.11	\$0.11
Total cost	**\$0.44**	**\$1.60**	**\$2.85**

Table S2. Material cost for fabricating the textile ESB.

Heat-sealable textile (\$14.95/1.67 yd^2)	\$2.14
Non-stick textile (\$13.95/1.67 yd^2)	\$0.58
Soft tubing (\$0.42/ft)	\$0.32
Total cost	**\$3.04**

Table S3. Material cost for fabricating the full textile-based energy harvesting system.

	6 mL	35 mL	72 mL
Heat-sealable textile ($14.95/1.67 yd^2)	$2.30	$2.69	$2.99
Non-stick textile ($13.95/1.67 yd^2)	$0.62	$0.73	$0.86
Polyurethane foam ($27.78/pint)	$0.13	$0.79	$1.61
Soft tubing ($0.42/ft)	$1.63	$1.63	$1.63
Check valves ($6.94 each)	$13.88	$13.88	$13.88
Total cost	**$18.56**	**$19.72**	**$20.97**

Table S4. Material cost for fabricating the arm-lift assistive device.

Heat-sealable textile ($14.95/1.67 yd^2)	$1.21
Non-stick textile ($13.95/1.67 yd^2)	$0.86
Soft tubing ($0.42/ft)	$0.28
Long sleeve compression shirt	$19.99
Sewing thread ($2.99/400 yd)	$0.01
Total cost	**$22.35**

Table S5. Material cost for fabricating the short and long supernumerary arms.

	Short (18 cm)	Long (30 cm)
Heat-sealable textile (\$14.95/1.67 yd^2)	\$0.33	\$0.57
Non-stick textile (\$13.95/1.67 yd^2)	\$0.06	\$0.12
Soft tubing (\$0.42/ft)	\$0.42	\$0.42
Check valves (\$6.94 each)	\$6.94	\$6.94
Soft silicone rubber gel (\$32.21/pint)	\$0.13	\$0.13
Total cost	**\$7.89**	**\$8.19**

Table S6. Maximum average power output of various foot-strike energy harvesting devices.

Device Type	Author, Year (Reference)	Peak Power Output
Electromagnetic	Hayashida, 2000 (*58*)	59 mW at 1 Hz
	Duffy, 2004 (*59*)	8.5 mW at 1 Hz
	Rao, 2013 (*60*)	0.3 mW at 4 km/h
	Shen, 2013 (*61*)	1.8 mW (walking)
	Xie, 2015 (*62*)	1.39 W at 5 km/h
	Purwadi, 2015 (*63*)	1.1 W at 7.2 km/h
	Ylli, 2015 (*64*)	0.84 mW at 6 km/h
	Xie, 2016 (*65*)	0.35 W at 7.2 km/h
	Wu, 2017 (*66*)	2.3 mW (running)
	Li, 2021 (*67*)	68 mW at 6 km/h
Piezoelectric	Shenck, 2001 (*68*)	8.4 mW at 1.1 Hz
	Howells, 2009 (*69*)	90.3 mW at 1 step
	Rocha, 2010 (*70*)	0.013 mW at 1 step
	Zhao, 2014 (*71*)	1 mW at 1 Hz
	Meier, 2014 (*72*)	2 μW (running)
	Jung, 2015 (*73*)	0.5 mW at 0.5 Hz
	Kalantarian, 2016 (*74*)	11.5 mW at 3250 steps
	Fan, 2017 (*75*)	0.35 mW at 8 km/h
	Turkmen, 2018 (*76*)	1.43 mW at 1 Hz
	Chaudhary, 2020 (*77*)	0.2 mW at 6 km/h
	Ramalingam, 2021 (*78*)	256 mW (walking)
	Wang, 2021 (*79*)	1.35 mW (theoretical)
	Jeong, 2021 (*80*)	52 μW at 1 step
Triboelectric	Hou, 2013 (*81*)	1.4 mW (peak)
	Zhang, 2015 (*82*)	4.9 mW (peak)
	Huang, 2015 (*83*)	2.1 mW at 1.8 Hz
	Haque, 2016 (*84*)	0.25 mW at 0.9 Hz
	Haque, 2018 (*85*)	0.28 mW (walking)
	Yun, 2021 (*86*)	2.6 mW at 1 Hz
	Yuan, 2021 (*87*)	1.35 mW at 3 Hz
	Wang, 2021 (*88*)	36 μW at 1.2 Hz
	Yao, 2021 (*89*)	213 μW at 5 Hz
	Gao, 2022 (*90*)	0.99 mW at 5 Hz (peak)
Tribo-piezo hybrid	Lee, 2020 (*91*)	127 μW (running)

Table S7. Characterization of the arm-lift assistive device. The table lists the angle of the upper arm with the vertical (top row) and the corresponding estimate for the lifting torque (bottom row) as a function of the input pressure to the arm-lift actuator and the weight suspended from the distal end of the arm.

		Weight suspended at the end of the arm (lbs.)						
		0	2.5	5	7.5	10	12.5	15
Actuator inflation pressure (bar)	0	9.31° 0.36 N m	5.34° 0.87 N m	0.57° 0.16 N m	1.71° 0.70 N m	3.20° 1.71 N m	2.79° 1.84 N m	4.67° 3.65 N m
	0.1	30.20° 1.11 N m	16.86° 2.70 N m	5.79° 1.66 N m	7.25° 2.97 N m	8.17° 4.36 N m	8.25° 5.42 N m	7.25° 5.66 N m
	0.2	38.91° 1.38 N m	23.78° 3.76 N m	14.92° 4.23 N m	11.57° 4.72 N m	11.66° 6.20 N m	11.08° 7.26 N m	10.91° 8.50 N m
	0.3	44.48° 1.54 N m	30.80° 4.77 N m	19.10° 5.38 N m	14.62° 5.94 N m	14.61° 7.74 N m	13.46° 8.79 N m	13.00° 10.10 N m
	0.4	47.87° 1.63 N m	33.91° 5.20 N m	23.06° 6.44 N m	17.71° 7.16 N m	16.82° 8.88 N m	15.88° 10.34 N m	15.33° 11.87 N m
	0.5	52.06° 1.73 N m	37.34° 5.65 N m	25.56° 7.09 N m	19.40° 7.82 N m	17.46° 9.20 N m	19.02° 12.31 N m	16.26° 12.57 N m
	0.6	55.88° 1.82 N m	39.78° 5.96 N m	29.47° 8.08 N m	20.17° 8.12 N m	22.89° 11.93 N m	19.42° 12.56 N m	17.84° 13.75 N m
	0.7	61.13° 1.92 N m	41.58° 6.18 N m	32.27° 8.77 N m	28.69° 11.31 N m	23.32° 12.14 N m	20.21° 13.05 N m	18.64° 14.35 N m
	0.8	62.89° 1.96 N m	43.75° 6.44 N m	34.92° 9.40 N m	29.29° 11.52 N m	24.84° 12.88 N m	22.71° 14.59 N m	20.38° 15.63 N m
	0.9	64.02° 1.98 N m	45.66° 6.66 N m	36.21° 9.71 N m	32.46° 12.64 N m	25.79° 13.34 N m	23.89° 15.30 N m	20.70° 15.87 N m
	1.0	65.05° 1.99 N m	46.18° 6.72 N m	36.36° 9.74 N m	32.74° 12.73 N m	26.08° 13.48 N m	24.17° 15.47 N m	21.54° 16.48 N m

Movie S1. Demonstration of the textile-based pneumatic energy harvesting system. The insole EHD harvests pneumatic energy as the user walks on a treadmill, which is stored in the wearable ESB.

Movie S2. Demonstration of the arm-lift assistive device. Pneumatic energy stored in the ESB (internal pressure of 1 bar) is utilized to actuate the arm-lift device, which abducts the shoulder joint of a mannequin arm.

Movie S3. Demonstration of the supernumerary robotic arm. Pneumatic energy stored in the ESB is utilized to operate the third arm device, enabling the user to pick up and move assorted objects on a table.

Data S1. (Separate file) Annotated MATLAB script implementing the mechano-fluidic model for the energy harvesting system.

Data S2. (Separate file) Vector design files used to laser pattern textile layers for fabricating the insole EHD, wearable ESB, and various assistive devices.